Journal of Cleaner Production 230 (2019) 910–926

Contents lists available at ScienceDirect

Journal of Cleaner Production

journal homepage: www.elsevier.com/locate/jclepro

Synthesis of zeolites from spent fluid catalytic cracking catalyst

Francesco Ferella*, Simona Leone, Valentina Innocenzi, Ida De Michelis, Giuliana Taglieri, Katia Gallucci

Department of Industrial and Information Engineering and Economics, University of L'Aquila, Via G. Gronchi 18, 67100 L'Aquila, Italy

ARTICLE INFO

Article history:
Received 24 July 2018
Received in revised form
14 May 2019
Accepted 15 May 2019
Available online 16 May 2019

Keywords:
FCC
Catalyst
Zeolite
Rare earths
Lanthanum
Cerium

ABSTRACT

The present paper describes the experimental tests for the recycling of fluid catalytic cracking catalysts (FCCCs). The process aims at the recovery of cerium (Ce) and lanthanum (La) as well as the reuse of the leaching solid residue that represents the actual problem in terms of global amount landfilled every year. Landfilling is still the main choice for the handling of such catalysts. This novel process proposes an alternative recycling approach that leads to the production of synthetic zeolites, that have several industrial applications. FCCC was leached by 1.5 mol/L of HNO_3, HCl and H_2SO_4 solutions at 80 °C, for 2 h with a solid to liquid ratio of 20 %wt, and the two rare earth elements were recovered by precipitation with an overall yield in the range 70–80%. The solid residues from the leaching stage were used as the base material for the synthesis of the zeolites by means of a combined thermal-hydrothermal treatment. The characterization of the zeolites demonstrated that the Na-A phase was predominant over the Na-X phase. The zeolites were tested as sorbent material for CO_2 separation from CH_4, in order to simulate the upgrading of biogas to biomethane. The maximum adsorption rate of CO_2 was 0.778 mol CO_2/kg of zeolite at 3 bar, with a resulting CH_4 recovery of 62% and 97 %vol as purity. Since the results in adsorption of CO_2 were not satisfying, the same zeolites were used to remove heavy metals from a synthetic wastewater solution containing three metals. Equilibrium and kinetic models were also developed in order to describe the adsorption process. The maximum adsorption load was calculated by the Langmuir isotherm and resulted to be 24–32 mg/g for Ni, 52–60 mg/g for Zn and 122–181 mg/g for Cu. The results also showed that the kinetics of the adsorption process is almost fast, as after 1 h at least 95% of zinc and copper were removed, whereas the kinetics of nickel was slower for all the three zeolites. As a conclusion, the zeolites are more efficient in metal adsorption than CO_2 capture, but other applications will be tested in the future.

1. Introduction

In the last fifty years, the significant expansion of the industrial, commercial and agricultural sectors was accompanied by a huge increase in production of petrochemical products and intermediates, as well as refined fuels like gasoline, diesel fuel, kerosene, jet fuel, naphtha, and gas oil. Hence, this led to massive use of catalysts for typical refinery processes like hydrotreating (HT), fluid catalytic cracking (FCC), catalytic reforming (CR), hydrodesulphurization (HDS), alkylation, isomerization. Many of them, once exhaust, can be regenerated by thermal treatments in presence of nitrogen, air or oxygen at a controlled temperature, but after a certain number of regenerations, the catalytic activity is irretrievably compromised. Other kinds of catalysts, like those for FCC, are poisoned by heavy metals such as nickel and vanadium, so that they cannot be regenerated and have to be replaced from time to time with fresh catalyst. The use of rare earths in FCC catalysts was driven by the need for more active and hydrothermally stable products with better yield performance. Rare earth oxides (REO) achieved these goals by enhancing catalytic activity and preventing the loss of acid sites during operation. REO concentration gradually increased over the years, and the average is currently in the range 3–5 %wt. China produces 95% of the world's rare earths elements (REEs) supply, thus the recovery of such elements from industrial waste will play a crucial role in the future economy of the European countries (BASF, 2018). It is difficult to quantify the real amount of FCCCs produced worldwide every year, as well as the relevant prices, since the main manufacturers like Grace Davison, Albemarle, Johnson Matthey, BASF, Haldor Topsoe, and Sinopec do not

* Corresponding author.
E-mail address: francesco.ferella@univaq.it (F. Ferella).

https://doi.org/10.1016/j.jclepro.2019.05.175
0959-6526/

release such data for free: they are published annually and the reports are very expensive (Ferella et al., 2016). Furthermore, the amount of spent FCCCs disposed of every year is also unknown. Nevertheless, some estimations were done in the last years (Letzsch, 2014). It is estimated that around 2300 tonnes of FCCCs are produced per day, equivalent to 840000 tonnes per year (Vogt and Weckhuysen, 2015).

Secondary REEs, mainly Ce, La, Y, Pr, Nd, Gd, and Sm, are also contained in phosphogypsum, that is the main by-product of the production of H_3PO_4 by H_2SO_4 digestion of phosphate rocks (Wu et al., 2018), or by using different strong acids (Walawalkar et al., 2016). Another waste that contains REEs is red mud, i.e. red tailings generated from the recovery of Al from primary ores: it contains Si, Al, Fe, Ca and Ti oxides and REEs, that can be extracted by leaching with mineral acids (Rao Borra et al., 2016) or, more efficiently, with ionic liquids (Davris et al., 2016). A review on the extraction of REEs from red mud was written by Liu and Naidu (2014).

Wang et al. (2017a) recovered La and Ce from FCC waste slag by leaching with HCl and selective precipitation of the REEs as $NaRE(SO_4)_2 \cdot xH_2O$ at pH 1 by means of Na_2SO_4. Al was recovered as $Al(OH)_3$ with the addition of NaOH at pH 4.5. The solid residue from leaching could be used as silica sources for some industrial applications. In another study, Wang et al. (2017b) leached FCC waste slag by a NaOH solution in order to convert Al into soluble $NaAlO_2$, that can be used as secondary raw material. The solid residue from the caustic leaching, containing the REEs and the remaining Al, was leached by HCl solution, from which Ce and La were precipitated by oxalic acid, and the resulting salt was calcined at 800 °C for 2 h to obtain the corresponding oxides. The total recovery of La and Ce was 97.6% and the grade was 98.7%, expressed as the concentration of the La_2O_3/CeO_2 mixture. The most used technique for extraction of REEs from leach liquors is solvent extraction: 2-ethylhexyl phosphoric acid-2-ethylhexyl ester (EHEHPA) in kerosene was used to recover La and Ce previously leached from spent FCCC by HCl. The recovery yields, for leaching, extraction, and stripping stages were 85, 100 and 96%, respectively (Ye et al., 2017). Di-(2-ethylhexyl) phosphoric acid (D2EHPA) extraction was also tested from HCl leach liquor, with an overall REEs recovery efficiency of 62.9% (Zhao et al., 2017). Ion-exchange is often used to extract REEs from leach liquors (Jha et al., 2016), for instance by polyacrylate anion-exchanger resin (Amberlite IRA 958) (Hubicka and Kołodyńska, 2001), chemically modified Amberlite XAD-4 (Dave et al., 2010), as well as resins containing mixed sulfonic/phosphonic, amino-phosphonic or iminodiacetic acid functional groups (Page et al., 2017). Bioleaching was also tested for an environmentally-friendly process: the maximum REE leaching yield was 49%, achieved by cell-free culture supernatants of *Gluconobacter oxydans*. The main organic acid detected in the medium was the gluconic acid, but the kinetics of the process is the constraining factor (Reed et al., 2016).

In a previous work, the comparison between direct precipitation and solvent extraction was studied for the recovery of Ce and La: H_2SO_4 was used as leaching medium, and Ce and La were recovered as sulphates by precipitation with NaOH: in fact, $NaRE(SO_4)_2 \cdot xH_2O$ are insoluble and can be easily precipitated at pH 2. In the second method, the FCCC was leached by HCl and the REEs were extracted by di-(2-ethylhexyl) phosphoric acid (D2EHPA), stripped with HCl and precipitated by oxalic acid (Innocenzi et al., 2015). Only one research group focused on the synthesis of zeolites from spent FCCC, whereas fly ash was largely used as a base material for production of synthetic zeolites (Koshy and Singh, 2016). Zeolites derived from fly ash were also tested for CO_2 adsorption and a future plant based on the upgrading of biogas into biomethane was assessed (Ferella et al., 2019a).

Nevertheless, LTA or 4A zeolite is a synthetic zeolite with a very small pore average diameter of 4 Å, that can be synthesized directly from fresh reagents like kaolin and soda ash and hydrothermal treatment at 70 °C for 2 h, followed by crystallization for 18 h at room temperature. Na-A zeolites are mainly used in gas purification, as ion exchanger in detergents, in catalysis and refinery processes. Regarding the price, the synthetic zeolites used as builders in detergents, for instance, are more competitive than phosphates and other sequestrants (Loiola et al., 2012). Na_2SiO_3 and $NaAlO_2$ were also used as precursors in the hydrothermal synthesis of zeolite LTA with a high degree of crystallinity (Garcìa Soto et al., 2013).

Few studies dealt with zeolite synthesis and characterization only from spent FCCCs. Hence, because of the aforementioned reasons, there is a clear gap in the state of the art relevant to the whole FCCC recycling: only one paper investigated the Cr^{3+} adsorption using a direct conversion of spent FCCC into zeolite, but with a different procedure and without recovering REEs. In fact, Na-A zeolite from spent FCCC was used to remove Cr^{3+} from aqueous solutions, and the solid obtained after the adsorption was mixed with cement mortars containing a fraction lower than 5% of such solid. Leaching tests showed that an effective immobilization of Cr^{3+} cations occurred (Gonzales et al., 2015).

Basaldella et al. (2006) tried to grind the spent FCCC before the hydrothermal treatment with NaOH solution. In that work, calcination at high temperature was not carried out and the zeolites obtained in this way were fully characterized. Na-X and mixed Na-X/Na-A zeolites were obtained with the particular hydrothermal procedure. Liu et al. (2012) synthesized zeolite Y with different particle sizes by means of FCCC fine powder. The results demonstrated that the cracking activity for heavy oil and resistance to coking of the fine zeolite catalysts were enhanced.

Basaldella et al. (2009) tested alkaline fusion with different $FCCC/Na_2CO_3$ ratios at 800 °C for 2 h, followed by hydrothermal crystallization with a 4 mol/L NaOH solution at 80 °C in presence of $NaAlO_2$. Conversion to Na-A (LTA) zeolite greater than 50% was obtained in all the crystallization tests. Spent FCC powder was also recycled together with Al waste foils as an aerating agent in the production of new geopolymer eco-cellular concrete (Font et al., 2017).

Spent FCCC was also used for the adsorption of hazardous phosphogypsum impurities. The addition of waste FCCC, in an amount not greater than 10 %wt, neutralized the acidity as well as regulated the phosphogypsum hydration. Additives modified the microstructure of hardened gypsum and enhanced its strength (Nizeviciene et al., 2016).

The current market prices do not justify the sole recovery of La and Ce from spent FCCC, as their concentration is rather low; nevertheless, REEs belong to the updated list of 27 critical raw materials released by the EU in 2017, so that their recycling becomes crucial in the close future (European Union, 2018).

The aim of the present work is to test a process that recovers the two rare earth elements (REEs) contained in the spent FCCCs and, at the same time, recycling the solid residue as raw material for manufacturing of synthetic zeolites, useful for many industrial applications. In particular, the zeolites were tested for CO_2 adsorption in the biogas upgrading process and adsorption of metals from one aqueous solution, and this represents the novelty of the work: many researchers tried to recover La and Ce with many different hydrometallurgical techniques, without studying any possible reuse of the solid residue.

2. Materials & methods

The paper was arranged as follows: spent FCCCs were firstly

characterized by several techniques, thus the REEs were extracted by a leaching stage with different acids. La and Ce were recovered from the leach liquors by ion-exchange and precipitation. The solid residues from the leaching stage were used to produce synthetic zeolites, that were tested in CO_2 adsorption and removal of metal ions from aqueous solutions. The research methodology is summarized in Fig. 1.

The characterization techniques for the spent FCCC sample, products and solutions are reported in the following subparagraphs, where the experimental trials are also explained in detail.

2.1. Characterization of spent FCCCs

The sample of the spent FCCC was supplied by Orim S.p.a. (Macerata, Italy). The sample was characterized in terms of metal content by X-ray fluorescence (XRF) (Spectro, Xepos) and inductively coupled plasma (ICP-OES, 5110 Agilent Technologies), X-ray diffraction (XRD, PANalytical X'Pert PRO), particle size distribution (PSD, Mastersizer 2000, Malvern), Brunauer-Emmet-Teller (BET) specific surface area (SSA, NOVA 1200e, Quantachrome porosimeter) and scanning electron microscopy (SEM, 20 kV Philips XL30 CP microscope).

2.2. Leaching tests

Three different inorganic acids were investigated: HCl, HNO_3 and H_2SO_4 at a constant concentration of 1.5 mol/L and fixed the solid to liquid (S/L) ratio equal to 200 g/L. These conditions were based on the results obtained in previous experiments so that the aim was to get as much extraction as possible with respect to the amount of acid. The temperature was kept constant at 80 °C. Lower values were not investigated since RE extraction yield enhanced significantly at the higher temperature (Innocenzi et al., 2015). The leaching trials were carried out in 250 ml screw flasks, in order to avoid excessive evaporation, immersed in a Dubnoff (ISCO) water bath with mechanical stirring at 200 rpm. For the preliminary leaching experiments, the reaction time was 3 h. Nevertheless, two samples were also taken after 1 and 2 h to figure out whether the longer reaction time would have justified a significant increase in the extraction of rare earths. All the samples were centrifuged at 5000 rpm to remove suspended particles, and diluted 1:10 with acidic water, in order to avoid precipitation of the elements during storage. The leaching trials were repeated twice. The concentration of Ce, La, Al, and Si in the leach liquors was determined by ICP-OES. The extraction yield was calculated as indicated in Ferella et al. (2017a).

2.3. Recovery of rare earths using ion exchange

These preliminary tests were carried out in order to extract selectively Ce and La from the leach liquor, by means of proper and selective adsorbent material. This stage has a double advantage: firstly, it allows to separate, although not completely, Ce and La from the other metals; secondly, such rare earths can be concentrated by using a small volume of diluted acid during the stripping step, obtaining a solution with a very low concentration of impurities.

Three resins and one granulated activated carbon (GAC, grain size 1–2 mm, Chemviron) were used as sorbents. In particular, Amberlite IRC 748, Amberlite IRC 86, Amberlite XAD 7HP resins were tested. Amberlite IRC 748 is an iminodiacetic acid chelating cation exchange resin with high selectivity for heavy metal cations over alkali metal ions. Amberlite IRC 86 resin is a gel type high capacity weak acid cation exchange resin containing carboxylic acid groups. Amberlite XAD 7HP is a non-polar resin generally used for adsorption of organic substances from aqueous systems and polar solvents. One chemically-modified Amberlite XAD-4 was already used for the extraction of La^{3+}, Nd^{3+}, and Sm^{3+} from a synthetic solution with quantitative results (Dave et al., 2010).

1 g of each sorbent was put in one beaker with 20 mL (S/L = 50 g/L) of solution coming from the leaching of spent FCCC with HCl. Three different pH values were tested: 2.9, that was the original pH of the leach liquor, 1 and 4, adjusted by means of 2 mol/L of HCl and NaOH solutions. This choice was due to the fact that strong cationic and chelating resins show the highest uptakes in an acidic pH range (Pasinli et al., 2005). pH values higher than 4 were not chosen to avoid precipitation of REEs.

One sample from each of the three leach liquors was taken in order to measure the concentration of metals, in particular Ce and La, together with Si and Al, that are the most concentrated impurities that could impair the adsorption of the rare earths.

Hence, twelve adsorption tests were carried out at 25 °C, under constant stirring at 200 rpm by a mechanical shaker (Innova 2000, New Brunswick). One sample was taken after 6 h and another one after 24 h, from each beaker. Those samples were centrifuged and diluted 1:10 with acidic distilled water for the analysis of metals by ICP-OES.

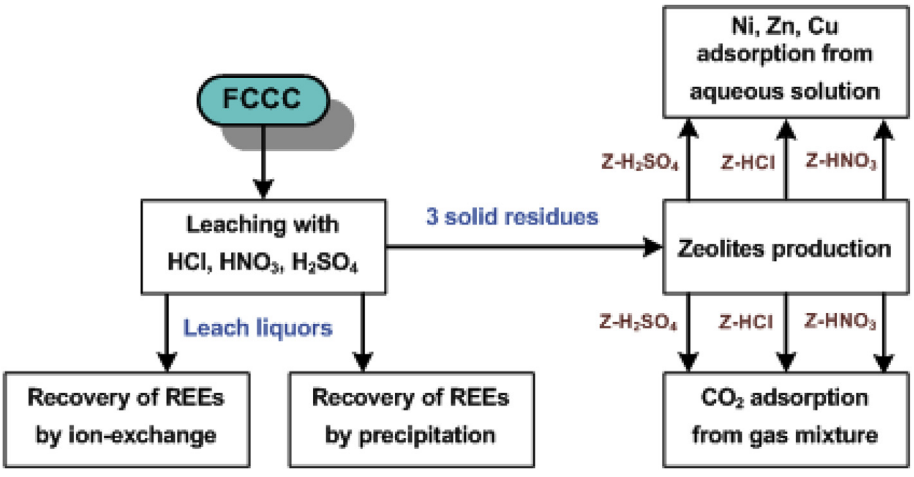

Fig. 1. Flow diagram for the overall experimental methods.

2.4. Recovery of rare earths by precipitation

Direct precipitation was the first method tested in order to separate Ce and La from the leach liquor. Tests were carried out with 100 mL of HCl and HNO_3 leach liquors, as REEs are almost unstable in sulphate solution and precipitate as soon as the pH increases slightly and/or the solution cools down (Innocenzi et al., 2015). Three different chemical agents were tested: H_3PO_4, Na_2CO_3, and $H_2C_2O_4$, added in an over-stoichiometric amount, calculated with respect to the concentration of Ce and La. The reactions lasted 1 h at 40 °C under magnetic stirring, after which the suspensions were filtered and one sample of each solution was taken for ICP analysis. These trials were done in order to take advantage of the low solubility of RE phosphates, carbonates and oxalates even at acidic pH values. All the three tests were carried out with HCl and HNO_3 leach liquors. Nevertheless, these tests did not give satisfactory results in terms of recovery and purity, as the RE precipitates were heavily contaminated by Al and Si, the most concentrated elements in the leach liquors.

For that reason, the first step of the recovery stage was to reduce the concentration of such impurities. Three recovery tests were carried out with HNO_3, HCl and H_2SO_4 leach liquors.

In the first trial, 500 mL of HNO_3 leach liquor containing 2370, 260, 375 and 11960 mg/L of La, Ce, Si, and Al at pH 0.87, were treated with 35 %wt NaOH solution at room temperature, under stirring for 30 min. The alkaline solution was added to increase the pH to 4. Such value was chosen in order to limit the simultaneous precipitation of REEs and iron. The test was conducted in a 1 L glass reactor. After that, the suspension was filtered by a 142 mm pressure filter system (Millipore YT30142HW). The solid was recovered, washed with distilled water and dried at 105 °C for 24 h. 2 mL sample was taken and diluted 1:10 with acid water for the ICP-OES analysis. The filtered solution was treated with a 50% over-stoichiometric amount (calculated with respect to the concentration of REEs) of oxalic acid at 40 °C for 1 h, under mechanical stirring. The reactions that take place are (1) and (2):

$$2\,Ce(NO_3)_3 + 3\,H_2C_2O_4 \rightarrow Ce_2(C_2O_4)_3 + 6\,HNO_3 \quad (1)$$

$$2\,La(NO_3)_3 + 3\,H_2C_2O_4 \rightarrow La_2(C_2O_4)_3 + 6\,HNO_3 \quad (2)$$

After cooling, the suspension was filtered again with the Millipore filter system; the solid, after washing with distilled water, was recovered and dried at 105 °C for 24 h and the solution analyzed for determination of metal content.

As regards the second test, 800 mL of HCl leach liquor was used. The initial concentration of La, Ce, Si, and Al in the solution was around 2560, 278, 280 and 12290 mg/L, respectively, at pH 2.22. The test was conducted in a 1 L glass reactor, at room temperature, with a mechanical stirrer equipped with an electric motor. 35 %wt NaOH solution was added slowly until pH 4 was achieved, and the suspension was left under stirring for 30 min. After that, the suspension was filtered by a 142 mm pressure filter system (Millipore YT30142HW). The solid was recovered, washed with distilled water and dried at 105 °C for 24 h. 2 mL sample was taken and diluted 1:10 with acidic water for ICP-OES analysis. The filtered solution was treated with a 50% over-stoichiometric amount (calculated with respect to the concentration of REEs) of oxalic acid at 40 °C for 1 h, under mechanical stirring. The reactions that take place are (3) and (4):

$$2\,CeCl_3 + 3\,H_2C_2O_4 \rightarrow Ce_2(C_2O_4)_3 + 6\,HCl \quad (3)$$

$$2\,LaCl_3 + 3\,H_2C_2O_4 \rightarrow La(C_2O_4)_3 + 6\,HCl \quad (4)$$

After cooling, the suspension was filtered again with the Millipore filter system; the solid was recovered, washed with distilled water and dried at 105 °C for 24 h and the solution analyzed for the determination of the metal concentrations.

In the last test with 500 mL of H_2SO_4 leach liquor, 33 %wt ammonia solution was added under stirring and room temperature as soon as the leach liquor was filtered, to avoid cooling and further precipitation of RE sulphates. The pH of the leach solution was 0.56; the concentration of La, Ce, Si, and Al was 2380, 260, 320 and 11930 mg/L, respectively. The final pH value of the solution was around 2 after the addition of ammonia. NH_4^+ ions cause the precipitation of ammonium alum. After 30 min, the solution was cooled down in order to lower the solubility of ammonium alum, thus the solid was filtered by the Millipore system. 2 mL sample was taken and diluted 1:10 with acidic water for the ICP-OES analysis. The solid was recovered and dried at 70 °C for 24 h, as its melting temperature is 95 °C. Oxalic acid was added in a 50% over-stoichiometric amount at 40 °C under mechanical stirring for 1 h, according to the reactions (5) and (6):

$$Ce_2(SO_4)_3 + 3\,H_2C_2O_4 \rightarrow Ce_2(C_2O_4)_3 + 3\,H_2SO_4 \quad (5)$$

$$La_2(SO_4)_3 + 3\,H_2C_2O_4 \rightarrow La_2(C_2O_4)_3 + 3\,H_2SO_4 \quad (6)$$

After cooling, the suspension was filtered again with the Millipore filter system; the solid was recovered and dried at 105 °C for 24 h and the solution analyzed for the determination of the metal concentrations. All the salts recovered after filtrations in the three tests were characterized by XRD, XRF or ICP-OES analyses.

2.5. Production and characterization of zeolites

Three different zeolites were synthesized from the solid residues coming from the leaching stage with HNO_3, HCl and H_2SO_4, accurately washed with distilled water in order to remove all the adsorbed caustic solution, until the water reached a pH value in the range 7–7.5. The synthesis procedure was similar to that used with fly ash in a previous work (Ferella et al., 2017b): two stages of the procedure were changed, in particular, the thermal treatment, that was carried out at 750 °C for 1.5 h, and the hydrothermal activation, that lasted 12 h at 95 °C. The zeolites were characterized by X-ray fluorescence (XRF) (Spectro, Xepos), X-ray diffraction (XRD) (PANalytical X'Pert PRO), Brunauer-Emmet-Teller (BET) specific surface area (SSA) (NOVA 1200e, Quantachrome porosimeter) and scanning electron microscopy (SEM) (20 kV Philips XL30 CP microscope) coupled with microanalysis. The zeolites were thus used to test their capacity in the adsorption of CO_2 from a CO_2/CH_4 gas mixture, simulating a typical biogas composition; such zeolites were also tested in the adsorption of metals, in particular, Ni, Zn and Cu from a synthetic acid solution.

2.6. CO_2 adsorption tests with zeolites

Zeolite Na-A could be selective for CO_2 adsorption because of the strong interactions between the quadrupole moment of CO_2 and the cations in the zeolite's structure (Mofarahi and Gholipour, 2014). Continuous dynamic trials were carried out in order to evaluate the sorption capacity of the three synthetic zeolites under typical industrial conditions. The arrangement of the lab-scale apparatus used for the CO_2 adsorption tests is shown in Fig. 2.

The experimental apparatus was made up of AISI 316 steel tubes, 2-, 3-way valves, mass flow controllers (MFCs A, B, C, and D), pressure indicators, one MFM (Mass Flow Meter) Bronkhorst High-Tech and two gas analyzers connected to a PC that recorded the data every 5 s. CO_2 and CH_4 were measured by means of a thermal

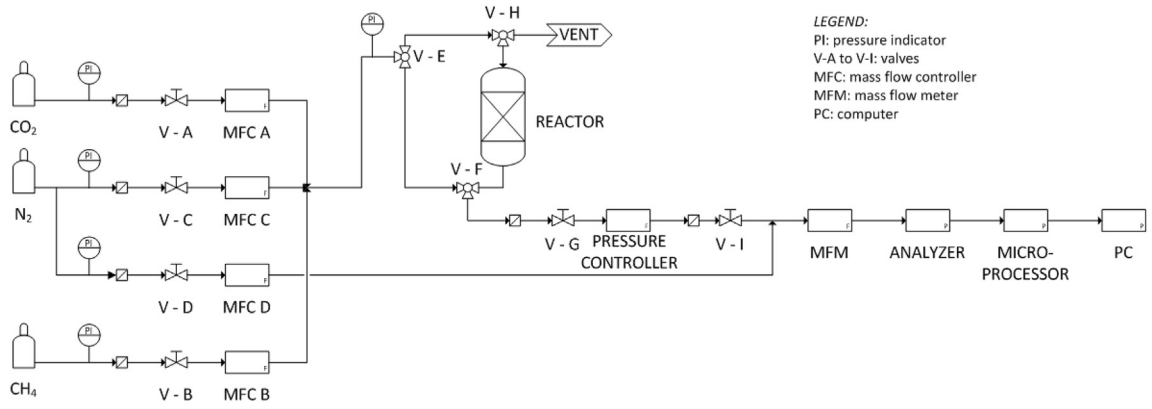

Fig. 2. Process flow diagram of the lab-scale plant.

conductivity analyzer (Uras-14, ABB). One Bronkhorst pressure reducer kept the pressure at the setpoint value. CH_4 and CO_2 were injected in the reactor through their own MFCs with a 100 mL/min full-scale capacity, in a ratio equal to 53/47 %vol., respectively, in order to simulate a real biogas mixture. N_2 was used for two purposes: as a diluting agent, since the gas analyzers need a minimum flow-rate of 1000 mL/min to work properly, and for post-adsorption washing, when the adsorbed CO_2 had to be stripped off after depressurization. Once mixed, the pressurized gas streams entered the fixed bed reactor consisting of an AISI 316L stainless steel tube of internal diameter of 0.91 cm and 80 cm length. Downstream the pressure reducer, the stream, diluted with N_2, passed through the MFM and then to the gas analyzers, whose concentration data were recorded by the software package WDA (Digipower s.r.l.).

Quartz wool and zirconia beads were used to distribute the gas flow throughout the cross-section of the reactor. The zeolite's fixed-bed height was 28 cm, corresponding to a mass of 18 g for each sample. The height of the fixed bed was calculated by Ergun's equation. The experimental procedure was already detailed in Ferella et al. (2017b). From Fig. 2, it is possible to notice that the gas flow can only be measured during the adsorption phase, i.e. when CO_2 is being adsorbed. During the desorption phase, when the system is suddenly depressurized to the ambient pressure, the measure of the CO_2 and the CH_4 contamination cannot be detected, so these data can only be evaluated by the material balance. Because of the aforementioned reasons, one first-order mathematical model with dead time flow distribution was proposed to determine the amount of the adsorbed CO_2 (Di Felice et al., 2011). During the adsorption phase, the total CH_4 recovery can be computed directly as indicated in Eq. (7):

$$CH_4^{out} = CH_4^{in} - CH_4^{ads} \tag{7}$$

Hence, knowing the total amount of CH_4^{in} injected (mol, measured before the test) and the amount that left the reactor (CH_4^{out} directly measured), it is possible to calculate the CH_4^{ads} adsorbed onto the zeolites, that shall be close to zero. The purity of CH_4 can be computed as in Eq. (8):

$$CH_4^{pur} = \frac{CH_4^{out}}{CH_4^{out} + \left(CO_2^{in} - CO_2^{ads}\right)} \tag{8}$$

The difference CO_2^{in}- CO_2^{ads} (mol) is the amount of CO_2 not adsorbed, and that thus contaminates the CH_4 recovered. On the other hand, the total CO_2 recovery can be calculated as indicated in Eq. (9):

$$CO_2^{ads} = CO_2^{in} - CO_2^{out} \tag{9}$$

whereas, the purity can be estimated as in Eq. (10):

$$CO_2^{pur} = \frac{CO_2^{ads}}{CO_2^{ads} + CH_4^{ads}} \tag{10}$$

In the ideal conditions, CH_4^{ads} is zero, so that the CO_2 purity is 1. This is very important as CO_2 can be a valuable by-product of the biogas separation plant, that could be liquefied and sold for many industrial purposes like beverage, fire extinguishers, metal inert gas welding, refrigeration, etc. When using the four formulas (7)–(10), the CH_4^{pur} was fixed to 97%, as the minimum value provided for by the Italian law for injection in the distribution grid is 95% (with CO_2 concentration ≤ 3 %vol.). Hence, the other three key parameters were calculated accordingly. Each term of the four formulas above can be calculated as integral of the mass flow rate of the gaseous compounds, with proper time edges (Ferella et al., 2017b).

2.7. Metal adsorption onto zeolites

Zeolites derived from fly ash have been used for removal of heavy metals and ionic species from urban and industrial wastewaters and spent solutions, acid mine drainage, removal of dyes and for leachate treatment. This wide use of zeolites is due to their ion exchange capacity and high uptake rate (Koshy and Singh, 2016). For that reason, the ion exchange capacity of the FCCC-derived zeolites was tested. The synthetic solution was prepared with 4.47 g of $NiSO_4 \cdot 6H_2O$, 3.92 g of $CuSO_4 \cdot 5H_2O$ and 4.40 g of $ZnSO_4 \cdot 7H_2O$ dissolved in 2 L of distilled water. The aforementioned amounts were calculated in order to have approximately a concentration of 500 mg/L for each Me^{2+} ion. The pH was adjusted to 3 by means of concentrated H_2SO_4 and NaOH solutions. 1 mL of such solution was taken, diluted 1:10 with acidic water and stored to measure the accurate concentration of the three metals.

Two different series of tests were conducted with zeolites: three kinetic and three equilibrium tests, the latter ones used for the determination of the maximum load of the sorbents. The kinetic tests were necessary in order to set the time after which the equilibrium of the adsorption process is reached. The kinetic tests were carried out by means of 100 mL of the synthetic solution containing Ni^{2+}, Zn^{2+} and Cu^{2+} ions put into contact with 2 g of zeolite, under stirring at 200 rpm in a mechanical stirrer (Innova 2000, New Brunswick), at room temperature (22 ± 1 °C). Samples were taken after 5′, 10′, 15′, 30′, 1 h, 2 h, 3 h, 4 h, 6 h, and 24 h. 1 mL of each sample was diluted 1:10 with acidic water and stored for

the analysis by ICP-OES.

The adsorption isotherms were determined by a batch contact of 1 g of each zeolite with ten different solutions at various concentrations (0.1–2 g/L for each metal ion, i.e. Ni, Zn, and Cu). The beakers were kept at room temperature and under mechanical stirring at 200 rpm for 24 h, when the equilibrium was achieved. Hence, the samples were taken and diluted 1:10 in order to measure the equilibrium metal concentrations (Pagnanelli et al., 2011). Two mathematical equations (Eq. (11) and (12)) were used to fit the kinetic experimental data: the Lagergren's pseudo first order and the Ho-McKay's pseudo second-order kinetic models expressed as:

$$q_t = q_e \cdot \left(1 - e^{-k_1 t}\right) \tag{11}$$

$$q_t = \frac{k_2 \cdot q_e^2 \cdot t}{1 + k_2 \cdot q_e \cdot t} \tag{12}$$

where q_t is the mass of the metal adsorbed per mass of zeolite at a certain time, mg/g; q_e is the mass of the metal adsorbed per mass of zeolite at the equilibrium, mg/g; k_1 is the Lagergren's kinetic constant, 1/min; k_2 is the Ho-McKay's kinetic constant, g/mg min; t is time, min (Millar et al., 2016). The parameters of the two kinetic models were derived by the ordinary least squares method. Four different models were used to fit the experimental data for the equilibrium isotherm of each ion and zeolite: Freundlich, Langmuir, Redlich-Peterson, and Dubinin-Radushkevich, described in Yousef et al. (2016).

3. Results & discussion

3.1. Characterization of spent FCCC

The concentration of the main elements is listed in Table 1.

Ce and La, as well as Al and Si, that represent the most concentrated elements in FCCC and are dissolved in great amount during leaching, were also measured by ICP-OES. The latter analysis gave the following values: Al 31.75%, Si 19.46%, La 1.57%, Ce 0.19% by weight. Al concentration is double with respect to the XRF value; this difference is due to the XRF technique that is less accurate when measuring the elements with the lowest atomic numbers. It is easy to realize that the total concentration of REEs is lower than 2 %wt, so that the recovery, also considering the current metal prices, cannot be profitable. The XRD diffraction pattern of spent FCCC is shown in Fig. 3.

The main crystalline phase found in the FCCC sample was dealuminated zeolite Na–Y; the other minor phases were zeolite ZSM-5 and alumina (Li et al., 2015). ZSM-5, a pentasil zeolite, composed of five-membered rings, is often used as a support material for catalysts. The Na–Y faujasite framework consists of sodalite cages which are connected through hexagonal prisms. Si/Al ratio is usually 2.43, but part of the alumina can be removed from the framework, resulting in a high-silica Na–Y zeolite, that indeed is used in cracking and hydrocracking catalysts. The particle size distribution was represented by a Gaussian curve centered at 80.4 μm, that is the D_{50}, whereas the Sauter's diameter D [3,2] was 73.6 μm.

Regarding the BET analysis, the SSA was nearly 112 m^2/g, not so lower than the SSA of a fresh FCCC, that is 116–180 m^2/g (BASF, 2018). The SEM picture of the spent FCCC is shown in Fig. 4a.

It is possible to note the granular shape of the FCCC particles, mainly composed by zeolite Y. In the last three pictures, cubic crystals can be recognized in the synthetic zeolites: this is the typical morphology of Na-A particles. In Fig. 3c and d, some crystals with the typical octahedral structure of Na-X zeolite can be detected.

Table 1
XRF analysis of spent FCCC and the three zeolites.

Sample	Na	Concentration (%wt)								
		Al	Si	P	Ti	V	Fe	Ni	La	Ce
FCCC	–	15.60	12.30	0.13	0.47	0.050	0.25	0.03	2.30	0.16
Z-HNO_3	8.06	12.07	12.19	–	0.44	0.004	0.19	0.03	0.33	0.02
Z-HCl	8.24	11.93	12.27	–	0.45	0.005	0.20	0.03	0.35	0.03
Z-H_2SO_4	7.98	11.59	11.74	–	0.45	0.005	0.19	0.03	0.33	0.03

3.2. Leaching of Ce and La

The extraction yields obtained at different reaction times are listed in Table 2.

As it can be inferred from the results, the extraction of Ce and La with the HNO_3 solution is lower than the corresponding extractions achieved with HCl and H_2SO_4. In the latter case, at 3 h, the average extraction yields for Ce and La are around 73% and 81%. Hence, increasing the reaction time by one hour, the extraction yields of La and Ce, the most important metals we are interested in, do not enhance significantly, so that 2 h can be selected as optimum reaction time. H_2SO_4 yields are a bit lower than those achieved in a previous work when a lower S/L ratio (150 g/L) and a greater concentration of acid (2 mol/L) were used (Innocenzi et al., 2015). The extraction of Si and Al are very similar in all the leaching tests, nearly 1.1% and 20%, that correspond to around 200 mg/L and 11.5 g/L.

Unfortunately, such concentrations of Si and Al entail many problems in the following recovery stage for Ce and La. Both Si and Al are partially soluble in acidic solutions: the first one tends to form colloidal silica, whereas the second one is an amphoteric compound. Al concentration in FCCC is the highest among all so that although the extraction was low, the concentration in leach liquors was not negligible.

The presence of dissolved silica was confirmed by the turbidity of the pregnant solutions, that was hard to filter by a paper filter; the aging of leach liquors resulted in the formation of amorphous silica, either in the form of a colloid or silica gel. Si and hot H_2SO_4 form dissolved and colloidal silica particles (40–100 nm), as soluble silica is present as the monomer silicic acid $Si(OH)_4$, according to Eq. (13):

$$Si + 2H_2SO_4 \leftrightarrow SiO_2 + 2H_2O + 2SO_2 \tag{13}$$

Silica gel formation can be described by the simplified reaction (14):

$$nSi(OH)_4 \leftrightarrow (SiO_2)_n + 2nH_2O \tag{14}$$

Particles of SiO_2 sols consist of branched chains or tetrahedral ring SiO_2, linked by siloxane bonds = Si–O–Si = . On the surface of the colloidal particles, Si atoms connected with groups = Si–OH are retained. As a result of the dissociation, the surface of the particles has a negative charge. The structure of the SiO_2 micelles hydrosol can be represented by the formula indicated in Eq. (15):

$$\left\{m[SiO_2] \cdot nSiO_3^{2-} \cdot 2(n-x)H^+\right\} 2xH^+ \tag{15}$$

where SiO_3^{2-} ions are potential ions and 2 (n-x)H^+ ions adsorbed layer is that in an electrostatic field moves together with the kernel. 2xH^+ ions form diffusion layer micelles. 100–200 mg/L as SiO_2 is the solubility range of amorphous silica in acidic medium, depending on the experimental conditions. Silica polymerization

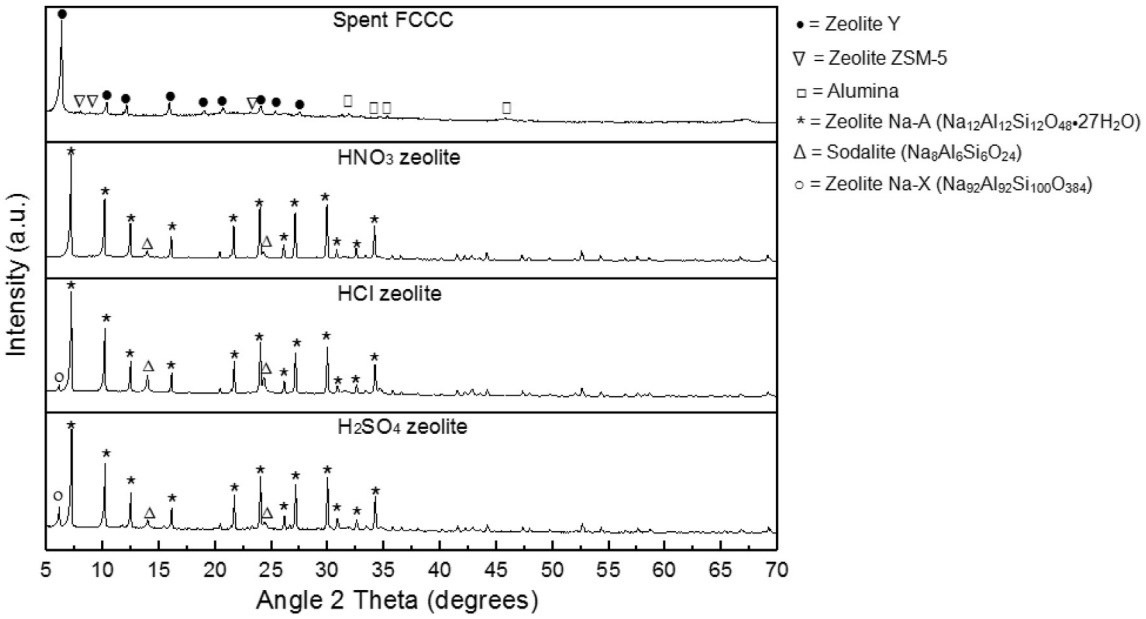

Fig. 3. XRD patterns of spent FCCC and the three zeolites synthesized from the leaching solid residues.

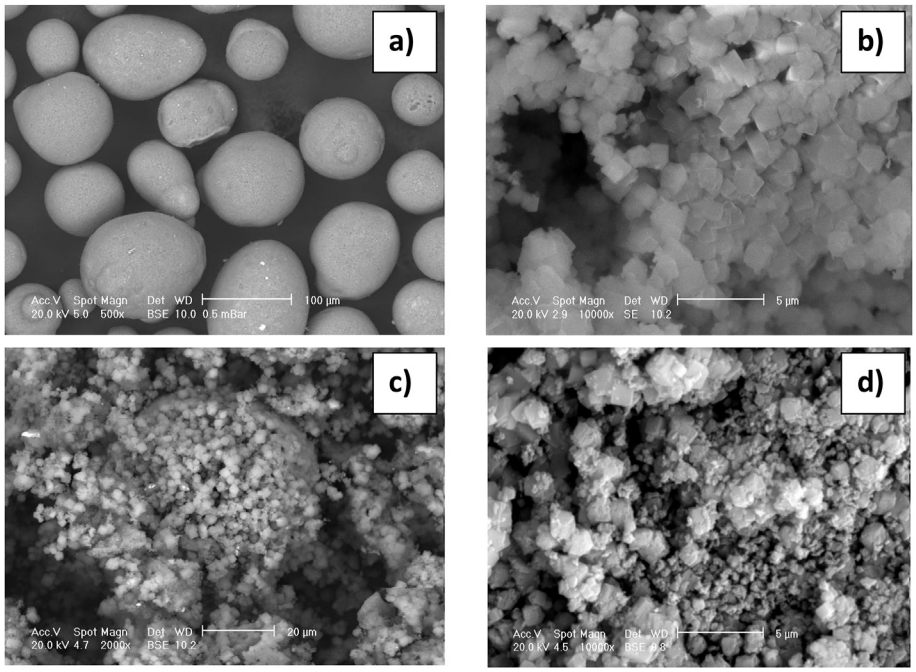

Fig. 4. SEM pictures of: a) spent FCCC; b) HNO_3 zeolite; c) HCl zeolite; d) H_2SO_4 zeolite).

reaction during leaching of metals are well described in the literature (Kazadi et al., 2016).

A double stage leaching process can be carried out to reduce the solubilization of Al and Si during treatment of FCCC waste slag: an alkali leaching with NaOH is able to extract $NaAlO_2$ and a subsequent leaching of the solid residue with HCl, added slowly in order to keep the pH around 1, minimizes the polymerization of silica and maximizes the extraction of REEs (Wang et al., 2017a).

Kamiya et al. (1974) demonstrated that the dissolution of Si is catalyzed by SO_4^{2-} as well as Cl^- ions and the catalytic activity of divalent SO_4^{2-} ions is higher than that of the monovalent Cl^- ions. The dissolution rate at 90 °C was accelerated between pH 2 and 4, and this effect was noticed with both HCl and H_2SO_4.

In this way, chloride and sulphate ions as catalysts promote the breakdown of chemical bonds in the SiO_2 structure. One method to suppress silica gel formation is the so-called "fuming pretreatment" with HCl and H_2SO_4, followed by the water leaching of the ore concentrate to recover REEs with extraction yields higher than 90%. In this method, silica precipitates in an insoluble form generating a filterable sludge in the subsequent water leaching stage (Davris et al., 2017).

Another similar way to control polymerization of silica is the water-starved system, able to reduce strongly silica solubilization and its subsequent polymerization during the leaching stage. Such

Table 2
Extraction yields of the leaching tests.

Sample	Extraction yield (%)			
	Ce	La	Si	Al
HNO_3 1 h	56.4 ± 2.1	61.5 ± 2.3	0.6 ± 0.2	14.9 ± 0.5
HNO_3 2 h	67.9 ± 1.6	76.6 ± 2.1	1.1 ± 0.1	18.4 ± 0.4
HNO_3 3 h	69.6 ± 2.5	78.8 ± 2.6	0.9 ± 0.1	19.4 ± 0.6
HCl 1 h	62.3 ± 2.1	69.8 ± 2.3	0.8 ± 0.2	16.7 ± 1.2
HCl 2 h	73.3 ± 3.0	81.5 ± 3.2	1.0 ± 0.2	21.4 ± 2.2
HCl 3 h	72.6 ± 3.1	80.4 ± 3.3	0.6 ± 0.2	20.6 ± 2.7
H_2SO_4 1 h	60.7 ± 1.3	72.6 ± 1.3	1.3 ± 0.1	17.0 ± 2.4
H_2SO_4 2 h	72.9 ± 2.5	80.4 ± 1.8	1.2 ± 0.1	19.8 ± 2.1
H_2SO_4 3 h	73.3 ± 2.2	82.1 ± 1.5	1.4 ± 0.2	22.7 ± 2.3

leaching is carried out with the aim to limit the amount of water during the leaching, in an acid excess condition, in order to limit the water available for the hydration of silica and then its polymerization. The dehydrated silica, instead, is readily filterable and can promptly be removed (Kazadi et al., 2016).

3.3. Recovery of rare earths using ion exchange

The results of the preliminary ion-exchange and adsorption tests are shown in Fig. 5.

As regards the REEs, the adsorption of Ce and La is clearly promoted by the lowest pH, i.e. 1. All the sorption yields after 24 h are higher than those at 6 h, and this took place at all the pH values for the four elements. Moreover, this trend can be recognized for all four sorbents. Nevertheless, the increase in the sorption yield is always lower than 10% from 6 to 24 h, so that the contact time could be optimized by kinetics tests. The maximum sorption yields for Ce and La at pH 1 were around 38 and 36%, respectively, achieved by resin IRC 748 after 24 h. At the same time, extractions of Si and Al were 38 and 17%, that are not so low considering their concentration in the leach liquor with respect to the amount of the REEs. There is not so much research about the adsorption of Ce and La, contained in real leach liquors, onto activated carbon and the three resins studied in this paper. For instance, adsorption isotherms for Amberlite IRC 86 were obtained with synthetic solutions of organic acids containing most of the REEs as chlorides, including La^{3+} and Ce^{3+}, in presence of Fe^{3+} and Al^{3+} ions. The optimal pH for extraction of La^{3+} was 4.38 in acetic acid medium, with a maximum uptake rate equal to 0.29 mmol/L. A similar result was obtained for Ce^{3+}, with a maximum extraction at pH 4.08 (Bezzina et al., 2018). Amberlite XAD 7 was able to extract 99% of La^{3+} ions contained in an acidic solution in 5 min at pH 3.5 and room temperature, but the uptake was greatly and positively enhanced by the impregnation with 2-ethylhexyl hydrogen 2-ethylhexyl phosphonate (Matsunaga et al., 2001). This study also found that the adsorption is promoted by higher pHs in the range 3–4.5. Adsorption of heavy metals onto AC can generally be attributed to ion exchange with carboxylic and phenolic hydroxyl functional groups. The adsorption capacity of AC was fostered by impregnation with specific chemicals, for instance, pentaethylenehexamine. The adsorption tests were carried out at room temperature with La^{3+} initial concentrations of 10–200 mM and an S/L ratio of 0.04 g/mL in HNO_3 medium at pH 4.5. Both original and impregnated AC were tested. The maximum adsorption capacity was 76.4 and 107.0 mg La/g of AC and impregnated AC, respectively. After four cycles, the La adsorption uptake of the impregnated AC did not decrease, while the desorption capacity fell from 84.4% to 70%. Desorption can be carried out by HNO_3 solution at pH 1 (Iannicelli Zubiani et al., 2018). Nevertheless, this research found that adsorption of La^{3+} onto AC is characterized by loss of uptake capacity with very acidic pH, that is in contrast with the

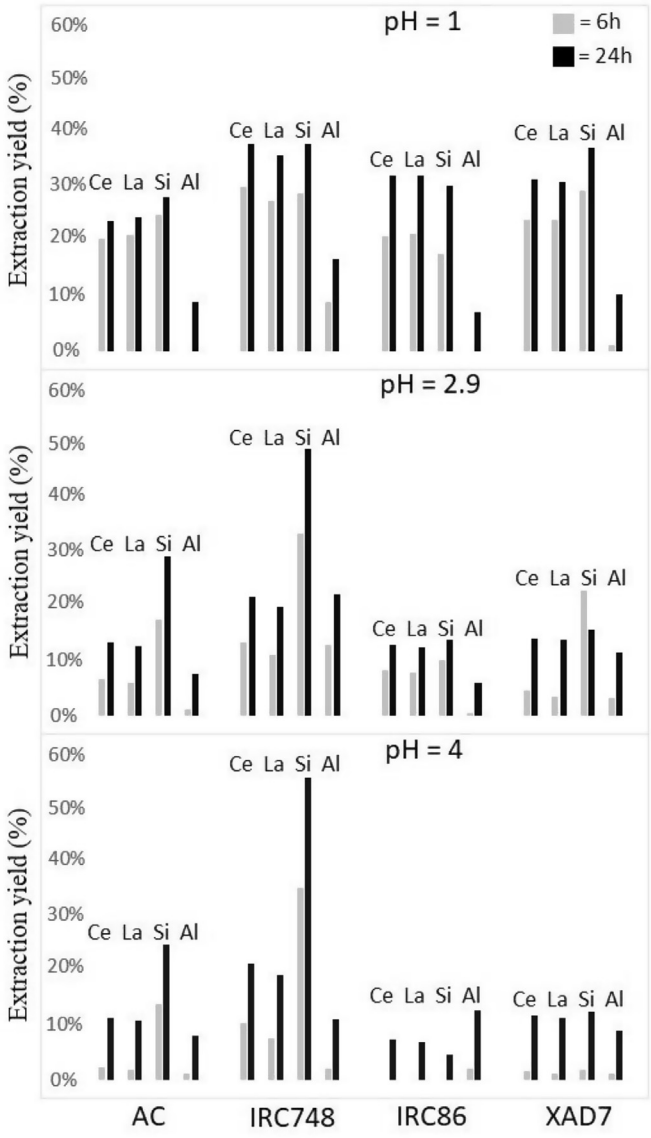

Fig. 5. Extraction yields for Ce, La, Si and Al from HCl leach liquor.

results found with our real solution. Several types of ACs, i.e. commercial, functionalized and recycled carbon black were tested in the adsorption of Y, La, Ce, Nd, and Sm from one acid synthetic solution. When compared with other carbon sorbent materials, the recycled tire carbon black demonstrated the largest adsorption of La and Ce, around 80 and 95% at 80 °C and pH 2. It was confirmed that the presence of other metal ions like zinc and magnesium lowers the adsorption of REEs (Smith et al., 2016).

Because of such results, it was decided not to study the adsorption kinetics and isotherm of the best adsorbent. In conclusion, the high concentration of Si and Al prevents the REEs from adsorbing completely onto the resins and the AC, since there is some sort of competition towards the active superficial sites of the solids. The results of the tests are not satisfactory in terms of total extraction and selectivity towards Ce and La.

Thus, it was necessary to reduce such interferences by using selective precipitation of Si and Al or solvent extraction of the REEs, before any use of selective adsorbents. After purification, ion-exchange could be tested again.

3.4. Recovery of rare earths by precipitation

These tests aimed at reducing the concentration of Si and Al in the leach liquors before the recovery of La and Ce. For that reason, the first stage of the recovery process was the removal of Si and Al. Solvent extraction by D2EHPA in n-heptane from HCl and HNO_3 leach liquors and the following precipitation of rare earths with oxalic acid gave the best results in terms of rare earths oxide grade, but such a method would be rather expensive at full scale considering the low concentration of La and Ce as well as the commercial price of the recovered oxide mixture (Innocenzi et al., 2015).

3.4.1. Test with HNO_3 leach liquor

The salt precipitated at pH 4 was a mixture of $Al(OH)_3$ and $NaNO_3$. Their concentration, according to the Reference Intensity Ratio (RIR) method, was 6% and 94 %wt. The latter reached its solubility product in those specific conditions and medium, whereas Al precipitates as hydroxide as the pH was getting increased; hence, other metals like iron, titanium, nickel, and vanadium, that anyway are already contained in very low concentration, mostly precipitated at pH 4. Looking at the concentration of Si in the solution after precipitation, it is clear that the salt also contains some Si, as around 16% co-precipitated after the addition of soda ash. Regarding REEs, there was a co-precipitation in the range of 2–4%. After precipitation with oxalic acid, only 1–2% of Ce and La remained into solution, and this confirmed that the precipitation was quantitative. The XRD analysis showed that the salt was a mixture of hydrated RE oxalates, i.e. $La_2(C_2O_4)\cdot 10H_2O$ and $Ce_2(C_2O_4)\cdot 9H_2O$.

The ICP-OES analysis of the RE concentrate showed the following concentrations: Al 0.1%, La 35.07%, Ce 3.50%, Na 0.87%, Fe 0.073% by weight. Si was negligible. Hence, the total recovery of Ce and La was around 69 and 76%, calculated with respect to their content in the FCCC's powder.

3.4.2. Test with HCl leach liquor

The salt precipitated by NaOH resulted to be a mixture of 86 %wt NaCl and 16 %wt $Al(OH)_3$, according to the XRD-RIR analysis. 90% of the Al contained in the leach solution precipitated. In this case, the amount of NaOH was lower than in the previous case as the original pH of the leach liquor was higher. 98% of Si precipitated but, because of the low concentration in the salt, no phases were detected by XRD analysis. The salt precipitated after the reaction with oxalic acid was a mixture of RE oxalates, as expected, like those precipitated from the HNO_3 leach liquor. The concentration of the elements in the RE oxalates, determined by ICP-OES, was the following: Al 0.44%, La 35.78%, Ce 2.79%, Na 2.60%, Fe 0.026% by weight. Si was negligible as in the previous case. The total recovery of Ce and La was equal to around 71 and 77%.

3.4.3. Test with H_2SO_4 leach liquor

In this trial, the 33 %wt NH_4OH solution was used in order to avoid precipitation of NaRE sulphates. The recovery of Al could represent another additional purpose of the process (Wang et al., 2017b). Ammonium aluminum sulphate dodecahydrate, also known as ammonium alum, with chemical formula $NH_4Al(SO_4)_2\cdot 12H_2O$, is a salt that precipitates at very acidic pH. $(NH_4)_2SO_4$ can also be used to provide NH_4^+ ions in order not to dilute the solution, and thus ammonia can be added to increase the pH. This selective precipitation is a viable way to recover a pure salt, as Al is very concentrated and must be removed in order to enhance the grade of the RE oxalate. The XRD spectrum of the salt is shown in Fig. 6.

Nearly 60% of Al was removed in this stage as ammonium alum, whereas no Si precipitated. The most probable phases in the salt precipitated after reaction with oxalic acid were $La_2(C_2O_4)\cdot 10H_2O$ and $Ce_2(C_2O_4)_3$, although the XRD spectrum was not crystalline. The total recovery was nearly 80% for both Ce and La. These values were a bit higher than those obtained in the previous two trials, as less REEs were lost during the precipitation of Al; such precipitation was indeed carried out at pH 2, lower than the pH value of the other two tests with HCl and HNO_3.

The salt recovered by oxalic acid was calcined at 600 °C for 2 h in the presence of air. The resulting oxide mixture was analyzed by ICP-OES, and the most concentrated elements were Al 0.028%, La 60.03%, Ce 6.52%, Fe 0.066% by weight. The concentration of the other elements was negligible.

3.5. Characterization of zeolites

The composition of the three zeolites is listed in Table 1, where the most concentrated and significant elements are reported only. The Si/Al ratio is always around 1, and this confirms that these are low silica synthetic zeolites. An increase in that ratio can significantly result in the enhancement of parameters like acid resistivity and thermal stability, whereas others like acid site density and cation concentration decrease.

The XRD spectra of the zeolites are shown in Fig. 3. The HNO_3 zeolite is composed of one main phase, that is hydrated zeolite Na-A with formula $Na_{12}Al_{12}Si_{12}O_{48}\cdot 27H_2O$ in a concentration of 92%, according to the Reference Intensity Ratio (RIR) method, plus 8% of Cl-free sodalite ($Na_8Al_6Si_6O_{24}$), another aluminosilicate mineral. Instead, the HCl zeolite is clearly composed of three phases: the same zeolite Na-A ($Na_{12}Al_{12}Si_{12}O_{48}\cdot 27H_2O$), Cl-free sodalite plus a third phase, that resulted to be dehydrated zeolite Na-X, with formula $Na_{92}Al_{92}Si_{100}O_{384}$. Zeolite Na-X is an ensemble of sodalite cages or β-cages joined by hexagonal prisms. More in depth, the crystalline structure is composed of stacking layers of sodalite cages joined by double-six rings in a tetrahedral arrangement, with a center of inversion at the center of the double-six rings (Lee et al., 2007).

Regarding the H_2SO_4 zeolite, it showed the same Na-A, Na-X and sodalite phases as for the sample coming from the HCl leaching residue. SEM pictures of the zeolites are shown in Fig. 4. Cubic crystals belong to the typical crystalline structure of zeolite Na-A (Loiola et al., 2012). In Fig. 4c, it can be recognized the growth of the Na-A crystals on one particle of the FCCC, whereas in Fig. 4b the crystallization process for zeolite Na-A achieved a higher grade. The morphology of Na-X crystals is in the form of octahedrons, composed of eight equilateral triangles (Lee et al., 2007), that can be seen in Fig. 4d, where a mixture of Na-A and Na-X phases is present, the latter in a lower concentration. The SSA for HNO_3, HCl and H_2SO_4 zeolite samples was around 12, 26 and 83 m^2/g, respectively. The complete characterization by BET and BJH analyses is reported in Table 3.

The value found for the Z-H_2SO_4 was by far the greatest among all: it is not simple to explain why such values are so different. Nevertheless, other authors obtained similar SSA values for Na-A zeolites, i.e. in the range 11–16 m^2/g (De C. Izidoro, 2013). Furthermore, it is well known that the zeolites produced from fly ash are characterized by SSA values ten-twenty times greater, as the Na-X phase is usually prevalent (Ferella et al., 2017b). One zeolite was also produced from spent FCCC without any preliminary leaching, using the same synthesis method: the SSA for that sample was 9.3 m^2/g: hence, the leaching treatment certainly enhances the SSA value, as the metal impurities like Fe, Ti, Ni, and V are mostly removed, but the main effect is the slight destabilization of the crystalline structure, due to the partial removal of Si and Al ions. This chemical action could have been more effective during the H_2SO_4 leaching, also taking into account the concentration of Si and

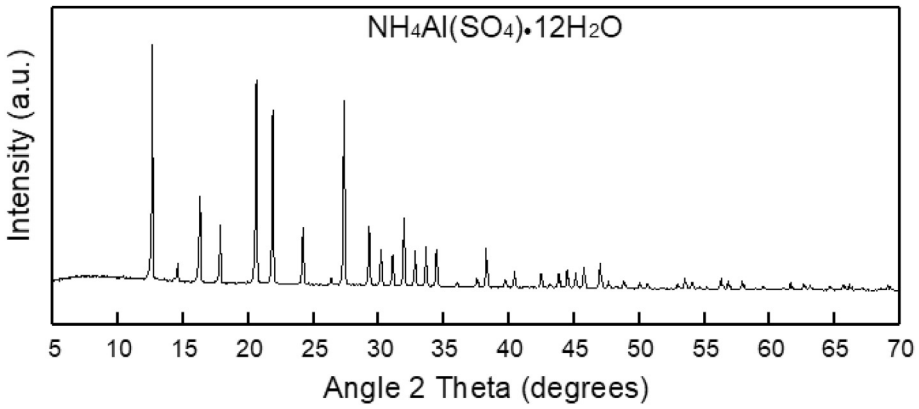

Fig. 6. XRD patterns of ammonium alum precipitated from H_2SO_4 solution.

Table 3
BET and BJH data of spent FCCC and zeolites.

Sample	BET (m^2/g)	BJH cumulative average pore volume (cm^3/g)	Average pore diameter ($4V_a/A$) (Å)
Spent FCCC	111.2	0.139	50
Z-HNO_3	11.8	0.030	102
Z-HCl	25.7	0.031	49
Z-H_2SO_4	83.2	0.062	30

Al for such zeolite (that is a bit lower than in the other two) and the extraction yields of Si and Al, that were indeed greater.

One previous work examined the effect of the three acids in the pre-treatment stage of the zeolite synthesis procedure, but the starting material was coal fly ash: the zeolites showed different SSA values ($HNO_3 < H_2SO_4 < HCl$) and pore volumes (0.12–0.80 cm^3/g), even though the average pore diameters were almost similar, i.e. in the range 4.17–4.34 Å (Panitchakarn et al., 2014).

3.6. Adsorption of CO_2

A typical diagram obtained in the tests is shown in Fig. 7, in particular from the trial with zeolite Z-HNO_3 at 3 bar. The adsorption process is carried out up to t^* (see Fig. 7), when the set-up purity of CH_4 is achieved (97%): after this time, the maximum CO_2 adsorption capacity of the zeolite is achieved, resulting in an increasing CO_2 concentration in the stream leaving the reactor. The fact that the red curve is shifted to the right with respect to the yellow curve (CH_4 blank) means that the methane is partially adsorbed by the zeolite (otherwise the two curves would have been overlapped). There is an increase in the concentration of CH_4 at the exit of the reactor, but this is the effect of the lower flow-rate due to the CO_2 that is trapped in the reactor. When the CO_2 starts exiting the reactor, the concentration of CH_4 goes back to the maximum, that is the same as the blank trial.

The performance of the three zeolites is shown in Fig. 8, where the results are reported in terms of recovery and purity of CO_2 and CH_4, that represents the most valuable product.

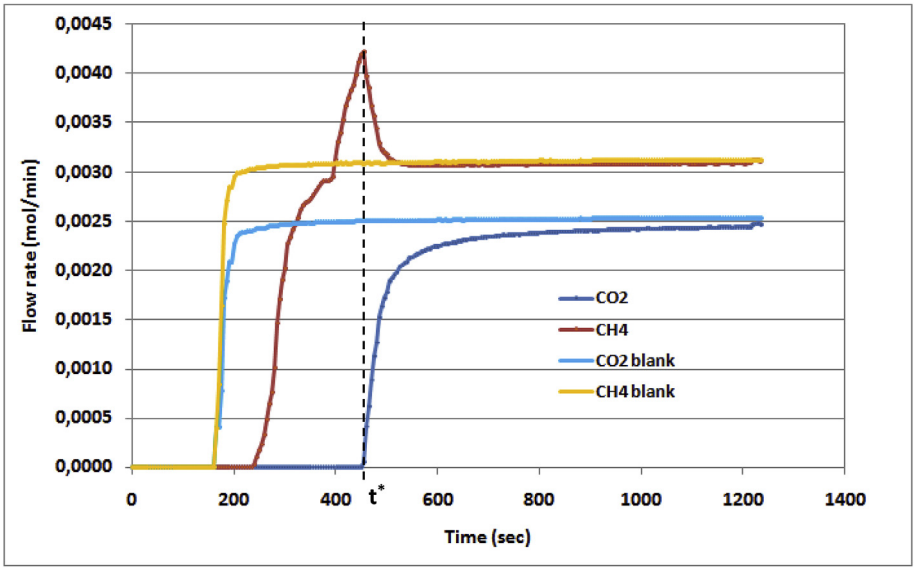

Fig. 7. CO_2/CH_4 mixture adsorption curves as a function of time (sample Z-HNO_3; p = 3 bar; T = 25 °C).

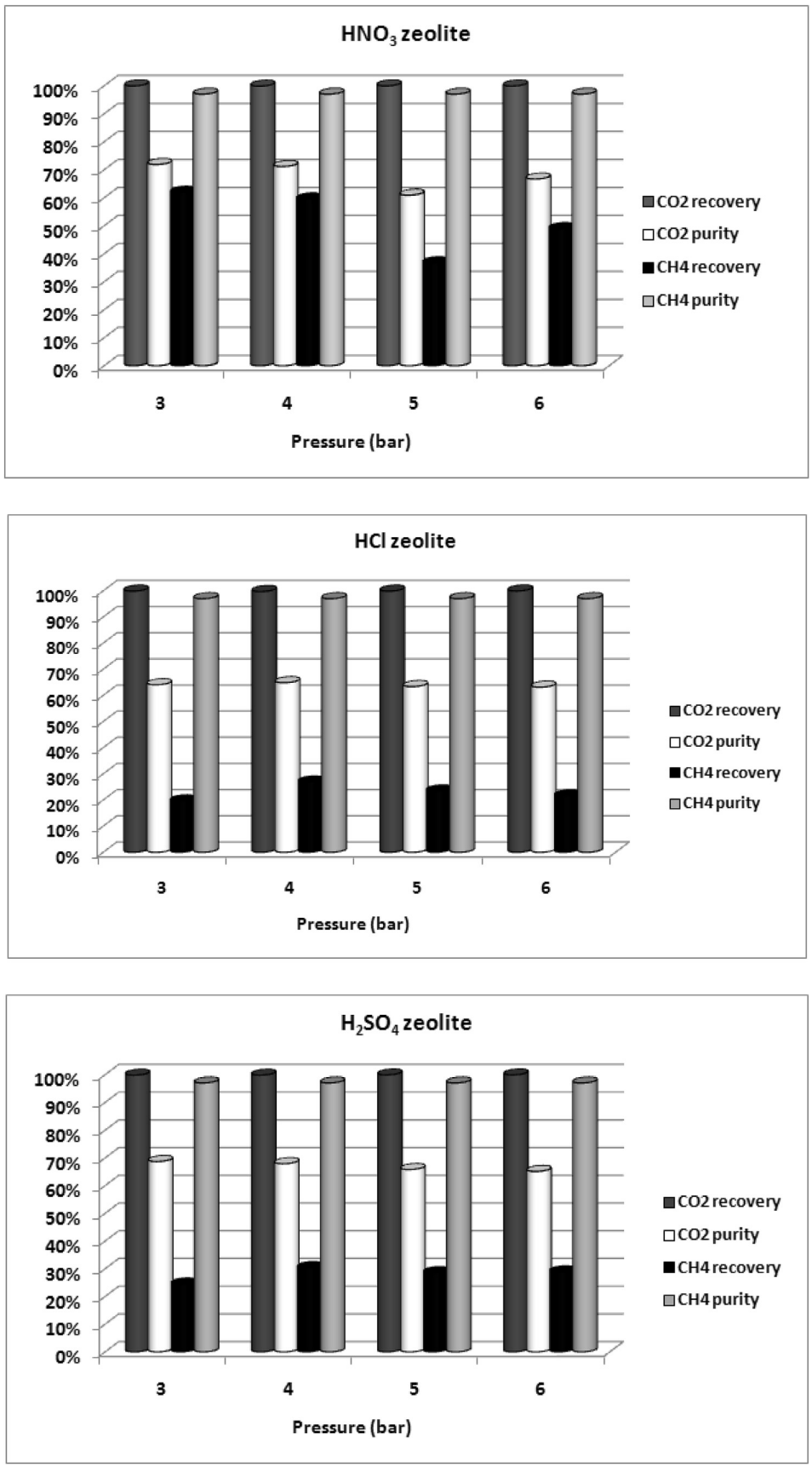

Fig. 8. Performance of the three zeolites in CO_2/CH_4 separation.

As it can be inferred from the graphs, the best results were obtained with HNO_3 zeolite at 3 bar: keeping fixed the CH_4 purity at 97%, the maximum recovery of CH_4 that can be achieved is only 62% of the total mass flowing through the reactor. This is due to the adsorption of part of CH_4 onto the zeolite, that is not very selective to CO_2. Such adsorbed CH_4 is released during the regeneration of the bed when the system is depressurized to ambient pressure and the CO_2 is stripped off from the zeolite: although the recovery of CO_2 is almost quantitative, the purity is rather low, around 72%. Hence, CO_2 cannot be reused as raw material, unless undergoes further treatment in order to increase its concentration. Alternatively, such a gas mixture can be burnt to supply thermal energy. As regards the specific adsorption rates, the experimental values are reported in Table 4.

The best performance was achieved by the HNO_3 zeolite at 3 bar, with 0.778 mol CO_2/kg zeolite that correspond to 34.2 g CO_2/kg zeolite. This is by far the greatest value achieved in the experimental tests. The specific adsorption rate decreased with pressure with the HNO_3 zeolite, whereas it increased with pressure with the other two samples (HCl and H_2SO_4 zeolites). Nevertheless, with the last two samples, the adsorption rate was lower than that achieved with HNO_3 zeolite for each pressure value. The different trend in adsorption of the CO_2 molecule cannot be directly attributed to the SSA, as such parameter was the lowest in the HNO_3 zeolite (12 m^2/g versus 26 and 83 m^2/g for HCl and H_2SO_4 zeolite). The main difference among samples lies in the crystalline structure, that is similar for HCl and H_2SO_4 zeolites (Na-A, Na-X, and sodalite), whereas the Na-X phase is missing in the structure of the HNO_3 zeolite.

Thus, what can be inferred by cross-checking the data is that the Na-A phase is able to adsorb CO_2 molecules more selectively over the CH_4 ones: in fact, with the other two zeolite samples, the recovery of CO_2 is always quantitative, but its purity is a bit lower: this means that more CH_4 was absorbed together with CO_2. What is very different is the amount of CH_4 recovered with the HCl and H_2SO_4 samples, that is very low compared to the recovery with the HNO_3 sample. This can be explained by the fact that the HCl and H_2SO_4 zeolites are saturated earlier by CO_2 and a small amount of CH_4 so that CO_2 is released from the bed and the recovery of CH_4 is inevitable lower, if the purity of 97% must be guaranteed. HNO_3 zeolite has the lowest SSA among all the three samples, but the adsorption of the CO_2 was the greatest. Hence, it might be possible that the pore distribution was centered on micropores in case of Z-HNO_3, that acts as a molecular sieve for CO_2 and CH_4 molecules. The kinetic diameter of CH_4 and CO_2 is 0.376 and 0.330 nm. Among all samples, Z-H_2SO_4 has a pore distribution with a greater concentration of micropores (defined as those pores with diameters not exceeding 20 Å, macropores are those with openings exceeding 500 Å and pores between 20 and 500 Å are called mesopores). Table 4 also lists the selectivity of the zeolites to CO_2, calculated by Eq. (16):

$$Selectivity = \frac{mol\ CO_2}{mol\ CH_4} \tag{16}$$

where the moles of the two gases are those adsorbed by the sorbent, so that the greater the selectivity, the better the zeolite is for biogas upgrading. It is clear that the highest selectivity is achieved by HNO_3 zeolite at 2 and 3 bar when the lowest amount of CH_4 was adsorbed. The tests were conducted at ambient temperature, but the selectivity increases with the temperature. The selectivity of the HNO_3 zeolite was in line with that predicted at those temperature and pressure levels by Mofarahi and Gholipour (2014), although they tested a commercial zeolite 5A under equilibrium conditions.

Table 4
Adsorption rate and selectivity of the zeolites.

	Adsorption rate (mol CO_2/kg zeolite)				Selectivity			
	3 bar	4 bar	5 bar	6 bar	3 bar	4 bar	5 bar	6 bar
Z-HNO_3	0.778	0.612	0.555	0.596	2.55	2.51	1.82	2.07
Z-HCl	0.271	0.276	0.315	0.367	0.55	0.72	0.75	0.75
Z-H_2SO_4	0.290	0.289	0.327	0.398	0.68	0.81	0.93	1.04

Comparing these results to those from fly ash zeolites obtained with a similar thermal/hydrothermal procedure, the main difference lies in the amount and grade of CH_4 obtained, as the selectivity was 2–4 times higher; correspondingly, also the grade and the recovery of CO_2 were higher than 98%. Instead, the results with FCC-zeolites are also similar to those obtained by granular activated carbon (Ferella et al., 2017b).

The only strong difference in the three samples was found in the crystalline structure formed during the thermal-hydrothermal crystallization procedure. HNO_3 zeolite does not show the Na-X phase, but only Na-A and sodalite crystals.

The recovery of CH_4 is just sufficient for the HNO_3 sample, but the CO_2 purity is not as high as required for further processing, so that must be burnt in the flare or, if possible, in a boiler where the heat can be useful for the self-consumption of the site.

Nevertheless, this study was based on a continuous dynamic study typical of the pilot- and full-scale applications: thus, it cannot be compared with results obtained by batch equilibrium tests.

3.7. Adsorption of metals

The parameters of the Lagergren and Ho-McKay models are listed in Table 5 for all the three metal ions.

Fig. 9 shows the experimental data for the adsorption of Ni, Zn and Cu onto the Z-HNO_3 as a function of time, and the kinetic models calculated according to Eqs. (11) and (12).

The other data obtained for Z-HCl and Z-H_2SO_4 were not reported graphically. The adsorption of Zn and Cu was usually very fast, as after 1 h at least 95% of the total amount of the ions were adsorbed by all the zeolites. After 24 h, more than 99% of the two metals were removed from the solution. Instead, the kinetics of Ni was slower, as after 1 h only 27% of the metal's mass was adsorbed by the Z-HNO_3 and Z-HCl. The Z-H_2SO_4 adsorbed around 44% of Ni after 1 h; after 24 h, Z-HNO_3, Z-HCl, and Z-H_2SO_4 adsorbed around 76%, 63% and 81% of Ni, respectively. Hence, Ni was the only metal that did not achieve quantitative adsorption. This trend can easily be recognized in Fig. 9a. Removal of metal ions from solution was more marked at very short contact times (Hashemian et al., 2013), and the addition of zeolite caused an increase in pH from 3 up to 6.23 for Z-HNO_3, 6.05 for Z-HCl and 6.22 for Z-H_2SO_4. These two phenomena were also observed in the work of Basaldella et al. (2007), in which a synthetic LTA zeolite was used for removal of Cr^{3+} ions. The increase in the final pH was also observed in the work of De C. Izidoro et al. (2013), where similar values (6.6–6.8) were achieved after adsorption of Cd^{2+} and Zn^{2+} by Na-A and Na-X zeolites.

Since the pHs after 24 h were lower than the typical values that cause precipitation of metals as hydroxides, the precipitation of Ni, Zn and Cu must be excluded. Thus, it can be inferred that the removal of metals was achieved by exchange and adsorption of metallic species. Since the initial pH is 3, the ion-exchange mechanisms, expressed by Eqs. (17) and (18) for the general metal ion can be supposed (Basaldella et al., 2007):

$$Z-Na + Me[H_2O]_6^{2+} \rightarrow Na^+ + Z-Me[H_2O]_6^{2+} \tag{17}$$

$$Z-Na + H^+ \rightarrow Na^+ + Z-H^+ \tag{18}$$

Table 5
List of the parameters calculated for Lagergren's and Ho-McKay's kinetic models.

Zeolite	Ion	Lagergren			Ho-McKay		
		q_e (mg/g)	k_1 (1/min)	R^2	q_e (mg/g)	k_2 (g/mg min)	R^2
Z-HNO_3	Ni^{2+}	16.84	0.008	0.862	18.36	0.00069	0.924
	Zn^{2+}	26.70	0.125	0.995	27.80	0.008	0.995
	Cu^{2+}	26.53	0.466	0.999	26.80	0.074	0.999
Z-HCl	Ni^{2+}	11.43	0.025	0.710	13.22	0.002	0.851
	Zn^{2+}	25.55	0.074	0.961	27.20	0.0039	0.995
	Cu^{2+}	26.29	0.250	0.974	26.95	0.0216	0.988
Z-H_2NO_4	Ni^{2+}	16.01	0.038	0.862	17.78	0.0026	0.940
	Zn^{2+}	26.56	0.132	0.999	27.46	0.0097	0.960
	Cu^{2+}	26.46	0.430	0.999	26.78	0.061	0.999

Me $[H_2O]_6^{2+}$ is the octahedral aqueous complex in the supercage, where Ni, Zn, and Cu ions are octahedrally coordinated. Thus, the neutralization of the solution is due to the uptake of H^+ by the zeolite's surface, that reduces the acidity of the medium. It is clear that the adsorbed amount of Ni was strongly affected by the presence of Zn and Cu competitor ions.

Zeolite Na-A has a pore size of 0.420 nm, that is very similar to those of the hydrated ionic diameters of Eq. (17): Ni $[H_2O]_6^{2+}$ 0.404 nm, Zn $[H_2O]_6^{2+}$ 0.430 nm, Cu $[H_2O]_6^{2+}$ 0.419 nm. Nevertheless, the size of the hydrated ions cannot explain the major affinity of the zeolites towards Zn and Cu: metal ions can form several aqueous species, that could have very different hydrated diameters. Hence, it may be possible that Ni formed different aqueous complexes with greater coordination number like Ni $[H_2O]_n^{2+}$, where $6 < n \leq 18$, that are the lowest energy structures but have greater ionic diameters. An alternative explanation could be that during the adsorption process, Zn and Cu ions lost more water molecules than the Ni ions, so the first two metals with a smaller ionic diameter filled in the zeolite's pores easily. A similar explanation was given in another work, that reported a higher Zn^{2+} adsorption rate over Cd^{2+} in a binary aqueous system (De C. Izidoro et al., 2013). Moreover, the zeolite network is anionic, but the surface charge of the zeolite particles in aqueous solution at a given pH depends on the zeolite isoelectric point (Basaldella et al., 2009). Gonzales et al. (2015) used 3 g of FCCC-derived zeolite, mainly composed of Na-A phase (80%) in 1 L of an aqueous solution containing 130 mg/L of Cr^{3+}. The synthetic zeolite was effective in adsorption of Cr, as the final concentration in the zeolite was 1.82 %wt as Cr_2O_3; this amount was greater than that adsorbed by a natural Na-A zeolite (1.60 %wt as Cr_2O_3). Nevertheless, the authors provided neither the unit adsorption rate nor the equilibrium results.

Redlich-Peterson and Dubinin-Radushkevich models were not useful to describe the equilibrium isotherms, as the experimental data were not fitted accurately, whereas the Freundlich and Langmuir equations were the most suitable to derive the isotherms. The theory on which the Langmuir model is based on implies that the sorption occurs at specific homogeneous surface sites of the sorbent, whereas in the Freundlich theory it is considered that the sorbent surface is heterogeneous and the adsorption process takes place with a non-uniform distribution of the reaction heat over the surface of the zeolite. The parameters of the Freundlich and Langmuir equations are reported in Table 6.

As it can be inferred from the correlation coefficient, the experimental data comply better with the Langmuir model than the Freundlich one. From the assessment of the equilibrium data, it is clear that the Z-H_2SO_4 had the best performance, as the maximum adsorption unit rate was the greatest for each metal ion.

It should be pointed out that these tests were carried out by a ternary ion system, although synthetic, and thus almost complex in terms of adsorption/ion-exchange phenomena. De C. Izidoro et al. (2013) studied a binary ion system with Cd^{2+} and Zn^{2+} in aqueous solution, using two synthetic Na-X and Na-A zeolites produced from fly ash. In this study, they demonstrated that zinc is preferentially adsorbed over cadmium in both single and binary systems under similar experimental conditions. The zeolite Na-A showed higher adsorption than the Na-X one. The adsorption isotherms were well described by the Langmuir model. The unit adsorption rates for Zn and Cd were 156–220 mg/g and 57–195 mg/g in the single and binary ion systems. The removal of both ions by Na-A was less affected by the presence of a competitive ion with respect to the Na-X zeolite.

This confirmed our results, as the adsorption isotherms were best fitted with the Langmuir model and showed the maximum simultaneous adsorption rate in the range of 24–32 mg/g for Ni, 52–60 mg/g for Zn and 122–181 mg/g for Cu. It is evidence of the experiments that with a greater concentration of metals, the exchange sites are filled earlier, with a resulting lower amount of single ions adsorbed onto the zeolites. The cation exchange capacity (CEC) is also important in such process, and this property is usually greater in Na-A than in Na-X based zeolites: this is due to the smaller Si/Al ratio in the framework of the zeolite Na-A, that causes a charge deficiency. This characteristic makes the Na-A zeolites more suitable in the adsorption of metal ions (De C. De C. Izidoro, 2013).

Nevertheless, it would also be interesting to determine the nature of the removal mechanisms of metal ions by such synthetic zeolites, but other specific analyses are required for both residual solutions and solids (Basaldella et al., 2007).

In the future, these zeolites could be tested as adsorbent material for separation of Ce and La from the leach liquors previously purified from Si and Al. A pH-edge study would be of great interest to figure out how the pH affects the adsorption of the synthetic zeolites.

4. Process analysis

From the analysis of the results obtained in the experimental tests, it was possible to design an integrated recycling process for spent FCCC. In particular, the final use of zeolite was chosen to be as an adsorbent of metals in wastewater treatment. It could also be used as a final treatment stage for produced water, in order to remove the small droplets of dispersed oil before reinjection into the oilfield wells. Regarding the leaching stage, H_2SO_4 was selected for two reasons: firstly, Al can be easily precipitated by ammonia, and this leads to a higher grade of the RE concentrate; secondly, the adsorption characteristics of the resulting zeolite are better than the other ones, in particular, the SSA and the maximum adsorption capacity.

Nevertheless, the fastest and economical way remains the direct precipitation of the REEs as $NaLa(SO_4)_2 \cdot nH_2O$ and

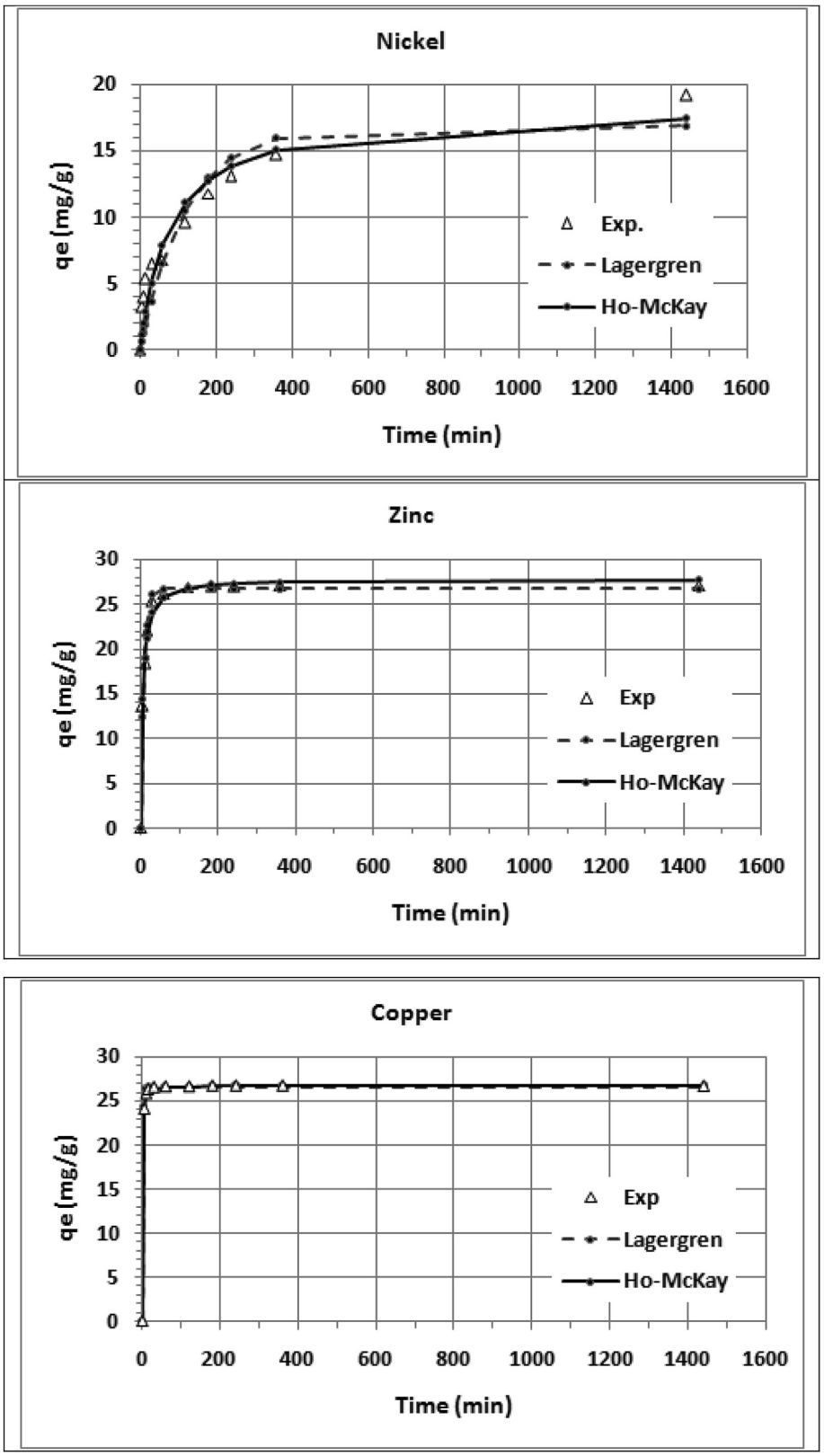

Fig. 9. Experimental data and kinetic models for the adsorption of Ni^{2+}, Zn^{2+}, and Cu^{2+} ions onto Z-HNO_3 (room temperature, pH = 3).

Table 6
Coefficients of the Freundlich and Langmuir isotherms.

Zeolite	Ion	Freundlich			Langmuir		
		K_F (mg/g) (L/mg)$^{1/n}$	1/n	R^2	q_m (mg/g)	K_L (L/mg)	R^2
Z-HNO_3	Ni^{2+}	11.325	0.156	0.656	29.103	0.218	0.951
	Zn^{2+}	26.901	0.118	0.930	52.860	0.537	0.966
	Cu^{2+}	11.941	0.360	0.984	122.503	0.018	0.946
Z-HCl	Ni^{2+}	11.552	0.126	0.820	24.713	0.162	0.921
	Zn^{2+}	19.138	0.181	0.871	54.400	0.284	0.929
	Cu^{2+}	31.769	0.262	0.984	143.378	0.103	0.986
Z-H_2NO_4	Ni^{2+}	13.419	0.167	0.864	32.257	0.240	0.990
	Zn^{2+}	26.714	0.145	0.941	60.188	0.528	0.913
	Cu^{2+}	25.043	0.335	0.982	181.170	0.051	0.946

$NaCe(SO_4)_2 \cdot nH_2O$, but one previous work demonstrated the poor quality of the RE concentrate due to the co-precipitation of Al (Innocenzi et al., 2015). RE oxalate mixture could be calcined to obtain RE oxides, increasing the concentration of Ce and La; nonetheless, such oxide alloy cannot be used as it is since it does not own any commercial application. Instead, it has to be dissolved again in acid in order to separate Ce and La by solvent extraction. Hence, after precipitation of ammonium alum at pH around 2, the REEs can be recovered by the addition of oxalic acid, and the pH of the solution remains below 2.5. This technical solution has the additional advantage of having a very acidic solution after the REEs recovery, and the spent solution can undergo regeneration for recovery of H_2SO_4, that is reused for the following leaching. This operation reduces greatly the operating costs. The flow-sheet of the entire recycling process is shown in Fig. 10.

One very effective method to remove colloidal silica and the remaining amount of Al and other salts is nanofiltration (NF) with special ceramic membranes: this technique is able to retain silica and aluminum salts in the retentate flow, whereas the acid passes through the membrane as permeate that can be reused for a further

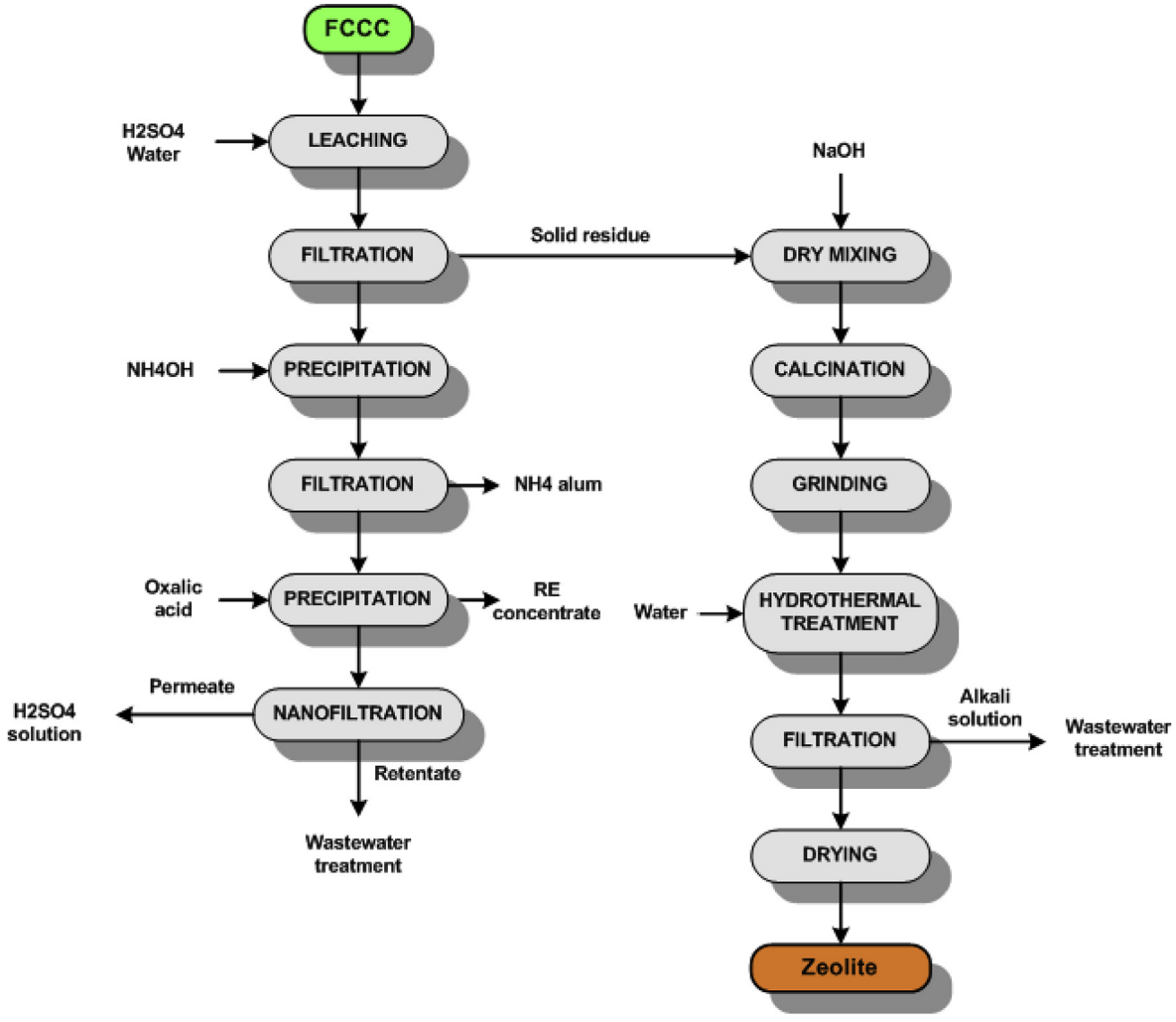

Fig. 10. Recycling flow-sheet for spent FCCC.

leaching stage.

Regeneration of the acid is crucial to make the reuse of spent FCCC viable, as the REEs content is very low. Although zeolites can be produced directly from spent FCC catalyst, the leaching stage is important in order to remove such metals that could be hazardous and may be released when using the resulting zeolite: in particular, Ni, V, and Ti.

An economic study was carried out to assess the profitability of a plant that treats 4000 tonnes per year of spent FCCC: the analysis showed that the unit production cost is 1.17 €/kg of synthetic zeolite. The detailed economic analysis is reported in another study (Ferella et al., 2019b).

The huge amount wasted every year in the world does not allow reuse of all the spent FCCC, even though part of the catalyst is currently used as a partial additive into cement and mortar powders. Nonetheless, this can certainly reduce the total amount of such catalyst annually disposed of in landfills, where it can undergo leaching by rainwater and pollute the groundwater table.

Natural and synthetic zeolites are extensively used in several applications and products thanks to their properties, for instance as a molecular sieve, catalyst, and ion-exchange medium. The natural zeolite segment was the greatest in 2014, accounting for over 60% of the global market volume. The synthetic zeolite demand has been tremendously increased over the past five years. The most requested synthetic zeolites are type-A, -Y, -X, and ZMS-5. They accounted for around 40% in 2014 but their market is expected to increase by the end of 2022. The petroleum industry is expected to be the primary sector that will drive growth over the forecast period. The global zeolite market was estimated at around USD 3.50 billion in 2014 and is expected to grow up to USD 4.50 billion in 2020, with 2 million tons of natural and synthetic zeolites produced globally (Grand View Research, 2018).

5. Conclusions

The sole recovery of Ce and La from spent FCCC is not profitable because of the low concentration of such REEs, so that a recycling process has to be coupled with the reuse and valorization of the solid residue coming from the leaching of the catalyst. The most useful way is the production of zeolites, that have a wide range of industrial applications. FCC catalyst was leached by 1.5 mol/L of HNO_3, HCl and H_2SO_4 solutions at 80 °C, for 2 h with an S/L ratio of 20 %wt. The best extractions and overall recovery yields for Ce and La were obtained with HCl and H_2SO_4 (72–80% and 73–82%). Some tests were carried out to recover Ce and La from the leach liquors. Ion-exchange tests with three different resins and AC did not give positive results because of the presence of high concentrations of Al and Si. The maximum recovery of Ce and La was indeed in the range 35–40% after 24 h with resin IRC748. Ce and La were instead recovered by selective precipitation with oxalic acid, after purification of the leach liquor by precipitation with alkaline reagents. The overall yield for both REEs was 70–80%.

The synthetic zeolites were used as a sorbent for metal removal from an acidic ternary synthetic solution containing Ni^{2+}, Cu^{2+}, and Zn^{2+} ions. The Langmuir isotherm resulted to be the more appropriate to fit the experimental data, and the maximum sorption capacity for the three zeolites was determined in the range 24–32 mg/g for Ni, 52–60 mg/g for Zn and 122–181 mg/g for Cu. The kinetic batch tests demonstrated that the adsorption of more than 95% of Zn and Cu is achieved after 1 h, whereas more than 99% of such ions' mass was removed after 24 h. The Ni's kinetics was a bit slower as the total adsorbed amount was 62–81% after 24 h for all the three zeolites. The zeolites were also used as sorbent material for CO_2 separation from CH_4, in order to simulate the upgrading of biogas to biomethane. The maximum adsorption rate of CO_2 was 0.778 mol CO_2/kg of zeolite at 3 bar, with a resulting CH_4 recovery of 62% with 97 %vol as purity. Hence, the synthetic zeolites are much more appropriate for adsorption of metals in aqueous solutions. The technical feasibility of the production of the Na-A zeolite was demonstrated in this paper. In the future, additional tests will be carried out to investigate if such zeolites are effective in the treatment of the produced water coming from the upstream oil separators, in the perspective of a circular economy approach in the oil refining industry.

Funding

This research did not receive any specific grant from funding agencies in the public, commercial, or not-for-profit sectors.

Acknowledgments

Authors kindly acknowledge Mr. Marcello Centofanti, Ms. Fabiola Ferrante and Dr. Ludovico Macera for their precious work in the characterization of the samples.

References

Basaldella, E.I., Paladino, J.C., Solari, M., Valle, G.M., 2006. Exhausted fluid catalytic cracking catalysts as raw materials for zeolite synthesis. Appl. Catal. B Environ. 66, 186–191.

Basaldella, E.I., Vázquez, P.G., Iucolano, F., Caputo, D., 2007. Chromium removal from water using LTA zeolites: effect of pH. J. Colloid Interface Sci. 313, 574–578.

Basaldella, E.I., Torres Sánchez, R.M., Conconi, M.S., 2009. Conversion of exhausted fluid cracking catalysts into zeolites by alkaline fusion. Appl. Clay Sci. 42, 611–614.

BASF, 2018. Fluid catalytic cracking (FCC) catalyst optimization to cope with high rare earth oxide price environment. Technical note. Available online: http://www.catalysts.basf.com/p02/USWeb-Internet/catalysts/en/function/conversions:/publish/content/microsites/catalysts/prods-inds/process-catalysts/BF-9626_US_REAL_Technical_Note.pdf. (Accessed 8 March 2018).

Bezzina, J.P., Ogden, M.D., Moon, E.M., Soldenhoff, K.L., 2018. REE behavior and sorption on weak acid resins from buffered media. J. Ind. Eng. Chem. 59, 440–455.

Dave, S.R., Kaur, H., Menon, S.K., 2010. Selective solid-phase extraction of rare earth elements by the chemically modified Amberlite XAD-4 resin with azacrown ether. React. Funct. Polym. 70, 692–698.

Davris, P., Balomenos, E., Panias, D., Paspaliaris, I., 2016. Selective leaching of rare earth elements from bauxite residue (red mud), using a functionalized hydrophobic ionic liquid. Hydrometallurgy 164, 125–135.

Davris, P., Stopic, S., Balomenos, E., Panias, D., Paspaliaris, I., Friedrich, B., 2017. Leaching of rare earth elements from eudialyte concentrate by suppressing silica gel formation. Miner. Eng. 108, 115–122.

De, C., Izidoro, J., Fungaro, D.A., Abbott, J.E., Wang, S., 2013. Synthesis of zeolites X and A from fly ashes for cadmium and zinc removal from aqueous solutions in single and binary ion systems. Fuel 103, 827–834.

Di Felice, L., Foscolo, P.U., Gibilaro, L.G., 2011. CO_2 capture by dolomite particles in a gas fluidized bed: experimental data and numerical simulations. Int. J. Chem. React. Eng. A55 (9).

European Union, 2018. Available online: http://eur-lex.europa.eu/legal-content/EN/ALL/?uri=COM:2017:0490:FIN. (Accessed 2 February 2018).

Ferella, F., Innocenzi, V., Maggiore, F., 2016. Oil refining spent catalysts: a review of possible recycling technologies. Resour. Conserv. Recycl. 108, 10–20.

Ferella, F., Belardi, G., Marsilii, A., De Michelis, I., Vegliò, F., 2017a. Separation and recovery of glass, plastic and indium from spent LCD panels. Waste Manag. 60, 569–581.

Ferella, F., Puca, A., Taglieri, G., Rossi, L., Gallucci, K., 2017b. Separation of carbon dioxide for biogas upgrading to biomethane. J. Clean. Prod. 164, 1205–1218.

Ferella, F., Cucchiella, F., D'Adamo, I., Gallucci, K., 2019a. A techno-economic assessment of biogas upgrading in a developed market. J. Clean. Prod. 210, 945–957.

Ferella, F., D'Adamo, I., Leone, S., Innocenzi, V., De Michelis, I., Vegliò, F., 2019b. Spent FCC E-Cat: towards a circular approach in the oil refining industry. Sustainability 11, 113.

Font, A., Borrachero, M.V., Soriano, L., Monzò, J., Payà, J., 2017. Geopolymer eco-cellular concrete (GECC) based on fluid catalytic cracking catalyst residue (FCC) with addition of recycled aluminium foil powder. J. Clean. Prod. 168, 1120–1131.

Garcìa Soto, A.R., Rodrìguez Niño, G., Trujillo, C.A., 2013. Zeolite LTA synthesis: optimising synthesis conditions by using the modified sequential simplex method. Ing. Invest. 33, 22–27.

Gonzales, M.R., Pereyra, A.M., Zerbino, R., Basaldella, E.I., 2015. Removal and cementitious immobilization of heavy metals: chromium capture by zeolite-

hybridized materials obtained from spent fluid cracking catalysts. J. Clean. Prod. 91, 187–190.
Grand View Research Inc, 2018. Zeolite Market Size, Share & Trends Analysis Report by Product, by Application (Catalysts, Detergent Builders), by Region (North America, Europe, Asia Pacific, CSA, MEA), and Segment Forecasts, 2012 - 2022. Available online: https://www.grandviewresearch.com/industry-analysis/zeolites-market. (Accessed 10 December 2018).
Hashemian, S., Hosseini, S.H., Salehifar, H., Salari, K., 2013. Adsorption of Fe(III) from aqueous solution by Linde type-A zeolite. Am. J. Anal. Chem. 4, 123–126.
Hubicka, H., Kołodynska, D., 2001. Studies on application of polyacrylate anion-exchangers in sorption and separation of iminodiacetate rare earth element(III) complexes. Hydrometallurgy 62, 107–113.
Iannicelli Zubiani, E.M., Gallo Stampino, P., Cristiani, C., Dotelli, G., 2018. Enhanced lanthanum adsorption by amine modified activated carbon. Chem. Eng. J. 341, 75–82.
Innocenzi, I., Ferella, F., De Michelis, I., Vegliò, F., 2015. Treatment of fluid catalytic cracking spent catalysts to recover lanthanum and cerium: comparison between selective precipitation and solvent extraction. J. Ind. Eng. Chem. 24, 92–97.
Jha, M.K., Kumari, A., Panda, R., Kumar, J.R., Yoo, K., Lee, J.Y., 2016. Review on hydrometallurgical recovery of rare earth metals. Hydrometallurgy 165, 2–26.
Kamiya, H., Ozaki, A., Imahashi, M., 1974. Dissolution rate of powdered quartz in acid solution. Geochem. J. 8, 21–26.
Kazadi, D.M., Groot, D.R., Steenkamp, J.D., Pöllmann, H., 2016. Control of silica polymerisation during ferromanganese slag sulphuric acid digestion and water leaching. Hydrometallurgy 166, 214–221.
Koshy, N., Singh, D.N., 2016. Fly ash zeolites for water treatment applications. J. Environ. Chem. Eng. 4, 1460–1472.
Lee, H.J., Kim, Y.M., Kweon, O.S., Kim, I.J., 2007. Structural and morphological transformation of NaX zeolite crystals at high temperature. J. Eur. Ceram. Soc. 27, 561–564.
Letzsch, W., 2014. Global demand for catalytic technology increases. Available online: http://www.hartfuel.com/f.catalyst.html. (Accessed 10 March 2018).
Li, Y., Sun, H., Feng, R., Wang, Y., Subhan, F., Yan, Z., Zhang, Z., Liu, Z., 2015. Synthesis of ZSM-5 zeolite from diatomite for fluid catalytic cracking (FCC) application. Appl. Petrochem. Res. 5, 347–353.
Liu, X., Li, L., Yang, T., Yan, Z., 2012. Zeolite Y synthesis with FCC spent catalyst fines: particle size effect on catalytic reactions. J. Porous Mater. 19, 133–139.
Liu, Y., Naidu, R., 2014. Hidden values in bauxite residue (red mud): recovery of metals. Waste Manag. 34, 2662–2673.
Loiola, A.R., Andrade, J.C.R.A., Sasaki, J.M., da Silva, L.R.D., 2012. Structural analysis of zeolite NaA synthesized by a cost effective hydrothermal method using kaolin and its use as water softener. J. Colloid Interface Sci. 367, 34–39.
Matsunaga, H., Ismail, A.A., Wakui, Y., Yokoyama, T., 2001. Extraction of rare earth elements with 2-ethylhexyl hydrogen 2-ethylhexyl phosphonate impregnated resins having different morphology and reagent content. React. Polym. 49, 189–195.
Millar, G.J., Couperthwaite, S.J., Alyuz, K., 2016. Behaviour of natural zeolites used for the treatment of simulated and actual coal seam gas water. J. Environ. Chem. Eng. 4, 1918–1928.
Mofarahi, M., Gholipour, F., 2014. Gas adsorption separation of CO_2/CH_4 system using zeolite 5A. Microporous Mesoporous Mater. 200, 1–10.
Nizeviciene, D., Vaiciukynien, D., Vaitkevicius, V., Rudzionis, Z., 2016. Effects of waste fluid catalytic cracking on the properties of semi-hydrate phosphogypsum. J. Clean. Prod. 137, 150–156.
Page, M.J., Soldenhoff, K., Ogden, M.D., 2017. Comparative study of the application of chelating resins for rare earth recovery. Hydrometallurgy 169, 275–281.
Pagnanelli, F., Ferella, F., De Michelis, I., Vegliò, F., 2011. Adsorption onto activated carbon for molybdenum recovery from leach liquors of exhausted hydrotreating catalysts. Hydrometallurgy 110, 67–72.
Panitchakarn, P., Laosiripojana, N., Viriya-Umpikul, N., Pavasant, P., 2014. Synthesis of high-purity Na-A and Na-X zeolite from coal fly ash. J. Air Waste Manage. 64, 586–596.
Pasinli, T., Eroglu, A.E., Shahwan, T., 2005. Preconcentration and atomic spectrometric determination of rare earth elements (REEs) in natural water samples by inductively coupled plasma atomic emission spectrometry. Anal. Chim. Acta 547, 42–49.
Rao Borra, C., Mermans, J., Blanpain, B., Pontikes, Y., Binnemans, K., Van Gerven, T., 2016. Selective recovery of rare earths from bauxite residue by combination of sulfation, roasting and leaching. Miner. Eng. 92, 151–159.
Reed, D.W., Fujita, Y., Daubaras, D.L., Jiao, Y., Thompson, V.S., 2016. Bioleaching of rare earth elements from waste phosphors and cracking catalysts. Hydrometallurgy 166, 34–40.
Smith, Y.R., Bhattacharyya, D., Willhard, T., Misra, M., 2016. Adsorption of aqueous rare earth elements using carbon black derived from recycled tires. Chem. Eng. J. 296, 102–111.
Vogt, E.T.C., Weckhuysen, B.M., 2015. Fluid catalytic cracking: recent developments on the grand old lady of zeolite catalysis. Chem. Soc. Rev. 44, 7342–7370.
Walawalkar, M., Nichol, C.K., Azimi, G., 2016. Process investigation of the acid leaching of rare earth elements from phosphogypsum using HCl, HNO_3, and H_2SO_4. Hydrometallurgy 166, 195–204.
Wang, J., Huang, X., Cui, D., Wang, L., Feng, Z., Hu, B., Long, Z., Zhao, N., 2017a. Recovery of rare earths and aluminum from FCC waste slag by acid leaching and selective precipitation. J. Rare Earths 35, 1141–1148.
Wang, J., Xu, Y., Wang, L., Zhao, L., Wang, Q., Cui, D., Long, Z., Huang, X., 2017b. Recovery of rare earths and aluminum from FCC catalysts manufacturing slag by stepwise leaching and selective precipitation. J. Environ. Chem. Eng. 5, 3711–3718.
Wu, S., Wang, L., Zhao, L., Zhang, P., El-Shall, H., Moudgil, G., Huang, X., Zhang, L., 2018. Recovery of rare earth elements from phosphate rock by hydrometallurgical processes - a critical review. Chem. Eng. J. 335, 774–800.
Ye, S., Jing, Y., Wang, Y., Fei, W., 2017. Recovery of rare earths from spent FCC catalysts by solvent extraction using saponified 2-ethylhexyl phosphoric acid-2-ethylhexyl ester (EHEHPA). J. Rare Earths 35, 716–722.
Yousef, N.S., Farouq, R., Hazzaa, R., 2016. Adsorption kinetics and isotherms for the removal of nickel ions from aqueous solutions by an ion exchange resin: application of two and three parameter isotherm models. Desalin. Water Treat. 1, 1–14.
Zhao, Z., Qiu, Z., Yang, J., Lu, S., Cao, L., Zhang, W., Xu, Y., 2017. Recovery of rare earth elements from spent fluid catalytic cracking catalysts using leaching and solvent extraction techniques. Hydrometallurgy 167, 183–188.